Nonlocal dynamics of nanoscale structures: Part 2

Professor Sondipon Adhikari

Chair of Aerospace Enginering, College of Engineering, Swansea University, Swansea UK
Email: S.Adhikari@swansea.ac.uk, Twitter: @ProfAdhikari
Web: http://engweb.swan.ac.uk/~adhikaris

Universitlé Paris-Est Marne-la-Vallée
January 18, 2016

Swansea University
Prifysgol Abertawe

Outline of this talk

1. **Introduction**
2. **Axial vibration of damped nonlocal rods**
   - Equation of motion
   - Analysis of damped natural frequencies
   - Asymptotic analysis of natural frequencies
3. **Dynamic finite element matrix**
   - Classical finite element of nonlocal rods
   - Dynamic finite element for damped nonlocal rod
   - Numerical results and discussions
   - Summary of results
4. **Introduction to nano-sensors**
   - Classical one-dimensional nano-sensors
5. **One-dimensional nano-sensors**
   - Attached biomolecules as point mass
   - Attached biomolecules as distributed mass
6. **Two-dimensional nano-sensors**
7. **Conclusions**

Nonlocal continuum mechanics

- Only limited work on nonlocal elasticity has been devoted to the forced axial vibration of damped nanorods.
- Aydogdu [1] developed a nonlocal elastic rod model and applied it to investigate the small scale effect on the axial vibration of clamped-clamped and clamped-free nanorods.
- Filiz and Aydogdu [2] applied the axial vibration of nonlocal rod theory to carbon nanotube heterojunction systems.
- Narendra and Gopalkrishnan [3] have studied the wave propagation of nonlocal nanorods.
- Murmu and Adhikari [4] have studied the axial vibration analysis of a double-nanorod-system. Here, we will be referring to a nanorod as a nonlocal rod, so as to distinguish it from a local rod.

Nonlocal dynamics

- Several computational techniques have been used for solving the nonlocal governing differential equations.
  These techniques include Naviers Method [5], Differential Quadrature Method (DQM) [6] and the Galerkin technique [7].
- Recently attempts have been made to develop a Finite Element Method (FEM) based on nonlocal elasticity. The upgraded finite element method in contrast to other methods above can effectively handle more complex geometry, material properties as well as boundary and/or loading conditions.
- Pisano et al. [8] reported a finite element procedure for nonlocal integral elasticity. Recently some motivating work on a finite element approach based on nonlocal elasticity was reported [9].
- The majority of the reported works consider free vibration studies where the effect of non-locality on the eigensolutions has been studied. However, forced vibration response analysis of nonlocal systems has received very little attention.

Nonlocal dynamics

- Based on the above discussion, in this lecture we develop the dynamic finite element method based on nonlocal elasticity with the aim of considering dynamic response analysis.
- The dynamic finite element method belongs to the general class of spectral methods for linear dynamical systems [10].
- This approach, or approaches very similar to this, is known by various names such as the dynamic stiffness method [11–21], spectral finite element method [10, 22] and dynamic finite element method [23, 24].

Dynamic stiffness method

- The mass distribution of the element is treated in an exact manner in deriving the element dynamic stiffness matrix.
- The dynamic stiffness matrix of one-dimensional structural elements, taking into account the effects of flexure, torsion, axial and shear deformation, and damping, is exactly determinable, which, in turn, enables the exact vibration analysis by an inversion of the global dynamic stiffness matrix.
- The method does not employ eigenfunction expansions and, consequently, a major step of the traditional finite element analysis, namely, the determination of natural frequencies and mode shapes, is eliminated which automatically avoids the errors due to series truncation.
- Since modal expansion is not employed, ad hoc assumptions concerning the damping matrix being proportional to the mass and/or stiffness are not necessary.
- The method is essentially a frequency-domain approach suitable for steady state harmonic or stationary random excitation problems.
- The static stiffness matrix and the consistent mass matrix appear as the first two terms in the Taylor expansion of the dynamic stiffness matrix in the frequency parameter.

Nonlocal dynamic stiffness

- So far the dynamic finite element method has been applied to classical local systems only. Now we generalise this approach to nonlocal systems.
- One of the novel features of this analysis is the employment of frequency-dependent complex nonlocal shape functions for damped systems. This in turn enables us to obtain the element stiffness matrix using the usual weak form of the finite element method.
- First we introduce the equation of motion of axial vibration of undamped and damped rods.
- Natural frequencies and their asymptotic behaviours for both cases are discussed for different boundary conditions.
- The conventional and the dynamic finite element method are developed. Closed form expressions are derived for the mass and stiffness matrices.
- The proposed methodology is applied to an armchair single walled carbon nanotube (SWCNT) for illustration. Theoretical results, including the asymptotic behaviours of the natural frequencies, are numerically illustrated.

Equation of motion

The equation of motion of axial vibration for a damped nonlocal rod can be expressed as

$$EA\frac{\partial^2 U(x,t)}{\partial x^2} + \widehat{c}_1\frac{\partial^3 U(x,t)}{\partial x^2 \partial t} = \widehat{c}_2\frac{\partial U(x,t)}{\partial t} + \left(1 - (e_0 a)^2\frac{\partial^2}{\partial x^2}\right)\left\{m\frac{\partial^2 U(x,t)}{\partial t^2} + F(x,t)\right\} \quad (1)$$

- This is an extension of the equation of motion of an undamped nonlocal rod for axial vibration [1, 4, 25].
- Here EA is the axial rigidity, m is mass per unit length, $e_0 a$ is the nonlocal parameter [26], $U(x,t)$ is the axial displacement, $F(x,t)$ is the applied force, x is the spatial variable and t is the time.
- The constant $\widehat{c}_1$ is the strain-rate-dependent viscous damping coefficient and $\widehat{c}_2$ is the velocity-dependent viscous damping coefficient.

Response analysis

- Assuming harmonic response as

$$U(x,t) = u(x)\exp\left[\mathrm{i}\omega t\right] \tag{2}$$

and considering free vibration, from Eq. (1) we have

$$\left(1 + \mathrm{i}\omega\frac{\widehat{c}_1}{EA} - \frac{m\omega^2}{EA}(e_0 a)^2\right)\frac{d^2u}{dx^2} + \left(\frac{m\omega^2}{EA} - \mathrm{i}\omega\frac{\widehat{c}_2}{EA}\right)u(x) = 0 \tag{3}$$

- Following the damping convention in dynamic analysis [27], we consider stiffness and mass proportional damping. Therefore, we express the damping constants as

$$\widehat{c}_1 = \zeta_1(EA) \quad \text{and} \quad \widehat{c}_2 = \zeta_2(m) \tag{4}$$

where ζ_1 and ζ_2 are stiffness and mass proportional damping factors. Substituting these, from Eq. (3) we have

$$\frac{d^2u}{dx^2} + \alpha^2 u = 0 \tag{5}$$

Response analysis

- Here

$$\alpha^2 = \frac{\left(\omega^2 - \mathrm{i}\zeta_2\omega\right)/c^2}{\left(1 + \mathrm{i}\omega\zeta_1 - (e_0 a)^2\omega^2/c^2\right)} \tag{6}$$

  with

$$c^2 = \frac{EA}{m} \tag{7}$$

- It can be noticed that α^2 is a complex function of the frequency parameter ω.
- In the special case of undamped systems when damping coefficients ζ_1 and ζ_2 go to zero, α^2 in Eq. (6) reduces to

$$\alpha^2 = \frac{\Omega^2}{1 - (e_0 a)^2\Omega^2}$$

  where $\Omega^2 = \omega^2/c^2$, which is a real function of ω.
- In a further special case of undamped local systems when the nonlocal parameter $e_0 a$ goes to zero, α^2 in Eq. (6) reduces to Ω^2, that is,

$$\alpha^2 = \Omega^2 = \omega^2/c^2$$

Damped natural frequencies

- Natural frequencies of undamped nonlocal rods have been discussed in [1]. Natural frequencies of damped systems receive little attention. The damped natural frequency depends on the boundary conditions.
- We denote a parameter σ_k as

$$\sigma_k = \frac{k\pi}{L}, \quad \text{for clamped-clamped boundary conditions} \tag{8}$$

$$\text{and} \quad \sigma_k = \frac{(2k-1)\pi}{2L}, \quad \text{for clamped-free boundary conditions} \tag{9}$$

- Following the conventional approach [27], the natural frequencies can be obtained from

$$\alpha = \sigma_k \tag{10}$$

- Taking the square of this equation and denoting the natural frequencies as ω_k we have

$$\left(\omega_k^2 - \mathrm{i}\zeta_2\omega_k\right) = \sigma_k^2 c^2 \left(1 + \mathrm{i}\omega_k\zeta_1 - (e_0 a)^2\omega_k^2/c^2\right) \tag{11}$$

- Rearranging we obtain

$$\omega_k^2\left(1 + \sigma_k^2(e_0 a)^2\right) - \mathrm{i}\omega_k\left(\zeta_2 + \zeta_1\sigma_k^2 c^2\right) - \sigma_k^2 c^2 = 0 \tag{12}$$

Damped natural frequencies

This is a very generic equation and many special cases can be obtained from this as follows:

- *Undamped local systems:* This case can be obtained by substituting $\zeta_1 = \zeta_2 = 0$ and $e_0 a = 0$. From Eq. (12) we therefore obtain

$$\omega_k = \sigma_k c \tag{13}$$

  which is the classical expression [27].

- *Undamped nonlocal systems:* This case can be obtained by substituting $\zeta_1 = \zeta_2 = 0$. Solving Eq. (12) we therefore obtain

$$\omega_k = \frac{\sigma_k c}{\sqrt{1 + \sigma_k^2 (e_0 a)^2}} \tag{14}$$

  which is obtained in [1].

Damped natural frequencies

- *Damped local systems:* This case can be obtained by substituting $\zeta_1 = \zeta_2 = 0$. Solving Eq. (12) we obtain

$$\omega_k = \mathrm{i}\left(\zeta_2 + \zeta_1 \sigma_k^2 c^2\right)/2 \pm \sigma_k c\sqrt{1 - \left(\zeta_1 \sigma_k c + \zeta_2/(\sigma_k c)\right)^2/4} \tag{15}$$

Therefore, the decay rate is $\left(\zeta_2 + \zeta_1 \sigma_k^2 c^2\right)/2$ and damped oscillation frequency is $\sigma_k c\sqrt{1 - \left(\zeta_1 \sigma_k c + \zeta_2/(\sigma_k c)\right)^2/4}$. We observe that damping effectively reduces the oscillation frequency.

Damped natural frequencies

- For the general case of a nonlocal damped system, the damped frequency can be obtained by solving Eq. (12) as

$$\omega_k = \frac{\mathrm{i}\left(\zeta_2 + \zeta_1\sigma_k^2 c^2\right)}{2\left(1+\sigma_k^2(e_0 a)^2\right)} \pm \frac{\sigma_k c}{\sqrt{1+\sigma_k^2(e_0 a)^2}}\sqrt{1 - \frac{\left(\zeta_1\sigma_k c + \zeta_2/(\sigma_k c)\right)^2}{4\left(1+\sigma_k^2(e_0 a)^2\right)}} \quad (16)$$

- Therefore, the decay rate is given by $\frac{\left(\zeta_2+\zeta_1\sigma_k^2 c^2\right)}{2\left(1+\sigma_k^2(e_0 a)^2\right)}$ and the damped oscillation frequency is given by

$$\omega_{d_k} = \frac{\sigma_k c}{\sqrt{1+\sigma_k^2(e_0 a)^2}}\sqrt{1 - \frac{\left(\zeta_1\sigma_k c + \zeta_2/(\sigma_k c)\right)^2}{4\left(1+\sigma_k^2(e_0 a)^2\right)}} \quad (17)$$

It can be observed that the nonlocal damped system has the lowest natural frequencies. Note that the expressions derived here are general in terms of the boundary conditions.

Asymptotic natural frequencies

- We are interested in dynamic response analysis of damped nonlocal rods. As a result, behaviour of the natural frequencies across a wide frequency range is of interest.
- An asymptotic analysis is conducted here to understand the frequency behaviour in the high frequency limit. We first consider the undamped natural frequency given by Eq. (14).
- To obtain asymptotic values, we rewrite the frequency equation in (14) and take the mathematical limit $k \to \infty$ to obtain

$$\lim_{k\to\infty} \omega_k = \lim_{k\to\infty} \frac{c}{\sqrt{\frac{1}{\sigma_k^2} + (e_0 a)^2}} = \frac{c}{(e_0 a)} = \frac{1}{(e_0 a)}\sqrt{\frac{EA}{m}} \qquad (18)$$

- This is obtained by noting the fact that for $k \to \infty$, for both sets of boundary conditions we have $\sigma_k \to \infty$. The result in Eq. (18) shows that there exists an 'upper limit' of frequency in nonlocal systems.

Asymptotic natural frequencies

- This upper limit of frequency is an inherent property of a nonlocal system. It is a function of material properties only and independent of the boundary conditions and the length of the rod.
- The smaller the value of $e_0 a$, the larger this upper limit becomes. Eventually for a local system $e_0 a = 0$ and the upper limit becomes infinite, which is well known.
- We consider a SWCNT to illustrate the theory. An armchair (5, 5) SWCNT with Young's modulus $E = 6.85$ TPa, $L = 25$ nm, density $\rho = 9.517 \times 10^3$ kg/m^3 and thickness $t = 0.08$ nm is considered as in [28].

Axial vibration of a single-walled carbon nanotube

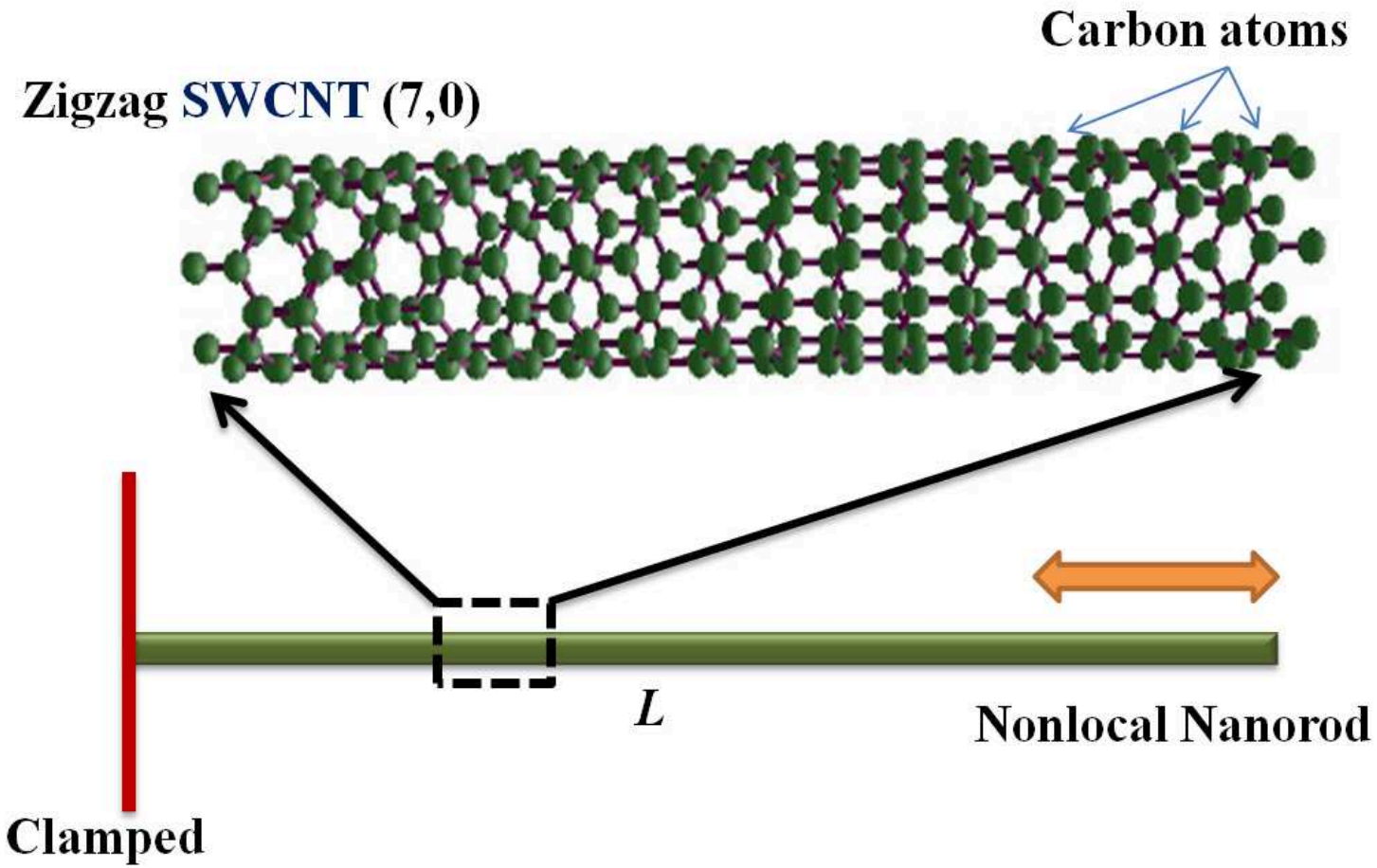

Figure: Axial vibration of a armchair (5, 5) single-walled carbon nanotube (SWCNT) with clamped-free boundary condition.

Nonlocal natural frequencies of SWCNT

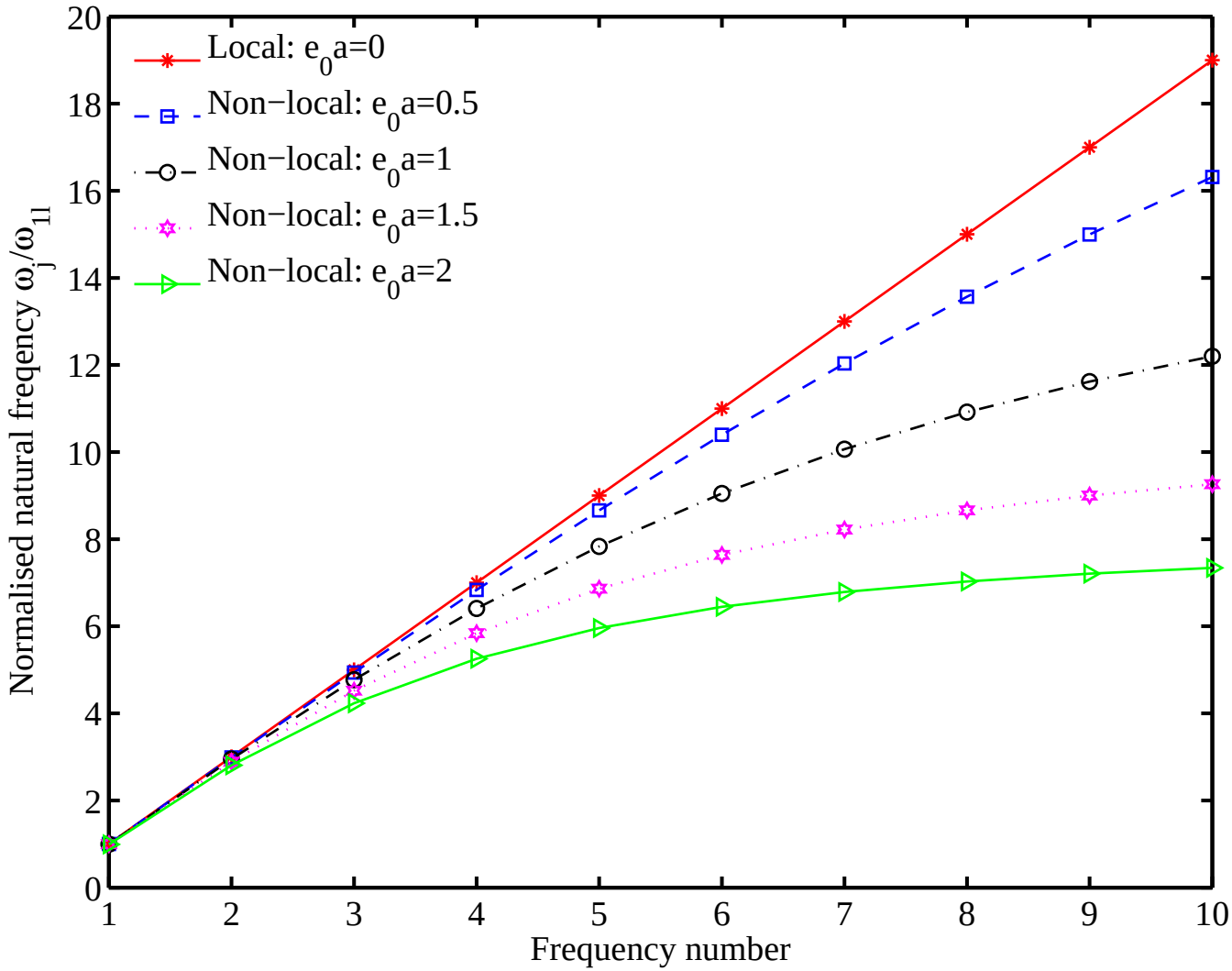

First 10 undamped natural frequencies for the axial vibration of SWCNT.

Asymptotic natural frequencies

- The frequency plot clearly shows that the natural frequencies decrease with increasing value of the nonlocal parameter $e_0 a$.
- One interesting feature arising for larger values of $e_0 a$ is that the frequency curve effectively becomes 'flat'. This implies that the natural frequencies reach a terminal value as shown by the asymptotic analysis
- Using Eq. (18), for large values of k, the normalised natural frequency plotted in the figure would approach to

$$\frac{\omega_k}{\omega_{1l}} \approx \frac{2/\pi}{(e_0 a/L)} \tag{19}$$

- Therefore, for $e_0 a = 2$ nm, we have $\omega_{k\max} \leq 7.957$. Clearly, the smaller the value of $e_0 a$, the larger this upper limit becomes.

Damped asymptotic frequency

- Now we turn our attention to the oscillation frequency of the damped system.
- Rewriting the expressions for the oscillation frequency from Eq. (17) and taking the limit as $k \to \infty$ we obtain

$$\lim_{k\to\infty} \omega_{d_k} = \lim_{k\to\infty} \frac{c}{\sqrt{\frac{1}{\sigma_k^2} + (e_0 a)^2}} \sqrt{1 - \frac{\left(\zeta_1 c + \frac{1}{\sigma_k^2}(\zeta_2/c)\right)^2}{4\left(\frac{1}{\sigma_k^2} + (e_0 a)^2\right)}}$$

$$= \frac{c}{(e_0 a)} \sqrt{1 - \left(\frac{\zeta_1 c}{2 e_0 a}\right)^2} \quad (20)$$

- Therefore the upper frequency limit for the damped systems is lower than that of the undamped system.
- It is interesting note that it is independent of the mass proportional damping ζ_2. Only the stiffness proportional damping has an effect on the upper frequency limit.

Asymptotic critical damping factor

- Equation (20) can also be used to obtain an asymptotic critical damping factor. For vibration to continue, the term within the square root in in Eq. (20) must be greater than zero.
- Therefore, the asymptotic critical damping factor for nonlocal rods can be obtained with $\lim_{k\to\infty} \omega_{d_k} = 0$ as

$$(\zeta_1)_{\text{crit}} = \frac{2e_0 a}{c} \tag{21}$$

- In practical terms, this implies that the value of ζ_1 should be less than this value for high frequency vibration.
- Again observe that like the upper frequency limit, the asymptotic critical damping factor is a function of material properties only and independent of the boundary conditions and the length of the rod.
- The asymptotic critical damping factor is independent of ζ_2.

Frequency spacing

- The spacing between the natural frequencies is important for dynamic response analysis as the shape of the frequency response function depends on the spacing.
- Because k is an index, the derivative $\frac{d\omega_k}{dk}$ is not meaningful as k is an integer. However, in the limit $k \to \infty$, we can obtain mathematically $\frac{d\omega_k}{dk}$ and it would mean the rate of change of frequencies with respect to the counting measure. This in turn is directly related to the frequency spacing.
- For the local rod it is well known that frequencies are uniformly spaced. This can be seen by differentiating ω_k in Eq. (13) as

$$\lim_{k\to\infty} \frac{d\omega_k}{dk} = c\frac{d\sigma_k}{dk}, \quad \text{where} \quad \frac{d\sigma_k}{dk} = \frac{\pi}{L} \tag{22}$$

for both sets of boundary conditions.

Frequency spacing

- For nonlocal rods, from Eq. (14) we have

$$\lim_{k\to\infty}\frac{d\omega_k}{dk} = \lim_{k\to\infty}\frac{d}{dk}\left(\frac{c}{\sqrt{\frac{1}{\sigma_k^2}+(e_0a)^2}}\right) = \lim_{k\to\infty}\frac{\pi}{L}\frac{c}{(\frac{1}{\sigma_k^2}+(e_0a)^2)^{3/2}\sigma_k^2}$$
$$= \lim_{k\to\infty}\frac{\pi}{L}\frac{c}{(e_0a)^3}\frac{1}{\sigma_k^2} = 0 \tag{23}$$

- The limit in the preceding equation goes to zero because $\sigma_k \to \infty$ for $k \to \infty$.
- This shows that unlike local systems, for large values of k, the undamped natural frequencies of nonlocal rods will tend to cluster together.
- A similar conclusion can be drawn by considering the damped natural frequencies also.

Classical finite element

- We consider an element of length ℓ_e with axial stiffness EA and mass per unit length m.

Figure: A nonlocal element for the axially vibrating rod with two nodes. It has two degrees of freedom and the displacement field within the element is expressed by linear shape functions.

- This element has two degrees of freedom and there are two shape functions $N_1(x)$ and $N_2(x)$. The shape function matrix for the axial deformation [29] can be given by

$$\mathbf{N}(x) = [N_1(x), N_2(x)]^T = [1 - x/L, x/L]^T \tag{24}$$

Classical finite element

- Using this the stiffness matrix can be obtained using the conventional variational formulation as

$$\mathbf{K}_e = EA \int_0^L \frac{d\mathbf{N}(x)}{dx} \frac{d\mathbf{N}^T(x)}{dx} \mathrm{d}x = \frac{EA}{L} \begin{bmatrix} 1 & -1 \\ -1 & 1 \end{bmatrix} \tag{25}$$

- The mass matrix for the nonlocal element can be obtained as

$$\begin{aligned} \mathbf{M}_e &= m \int_0^L \mathbf{N}(x)\mathbf{N}^T(x)\mathrm{d}x + m(e_0 a)^2 \int_0^L \frac{d\mathbf{N}(x)}{dx} \frac{d\mathbf{N}^T(x)}{dx} \mathrm{d}x \\ &= \frac{mL}{6} \begin{bmatrix} 2 & 1 \\ 1 & 2 \end{bmatrix} + mL(e_0 a/L)^2 \begin{bmatrix} 1 & -1 \\ -1 & 1 \end{bmatrix} \\ &= mL \begin{bmatrix} 1/3 + (e_0 a/L)^2 & 1/6 - (e_0 a/L)^2 \\ 1/6 - (e_0 a/L)^2 & 1/3 + (e_0 a/L)^2 \end{bmatrix} \end{aligned} \tag{26}$$

- For the special case when the rod is local, the mass matrix derived above reduces to the classical mass matrix[29, 30] as $e_0 a = 0$.

Dynamic finite element

- The first step for the derivation of the dynamic element matrix is the generation of dynamic shape functions.
- The dynamic shape functions are obtained such that the equation of dynamic equilibrium is satisfied exactly at all points within the element.
- Similarly to the classical finite element method, assume that the frequency-dependent displacement within an element is interpolated from the nodal displacements as

$$u_e(x,\omega) = \mathbf{N}^T(x,\omega)\widehat{\mathbf{u}}_e(\omega) \tag{27}$$

- Here $\widehat{\mathbf{u}}_e(\omega) \in \mathbb{C}^n$ is the nodal displacement vector $\mathbf{N}(x,\omega) \in \mathbb{C}^n$ is the vector of frequency-dependent shape functions and $n = 2$ is the number of the nodal degrees-of-freedom.

Complex shape functions

- Suppose the $s_j(x,\omega) \in \mathbb{C}, j = 1,2$ are the basis functions which exactly satisfy Eq. (5).
- It can be shown that the shape function vector can be expressed as

$$\mathbf{N}(x,\omega) = \mathbf{\Gamma}(\omega)\mathbf{s}(x,\omega) \tag{28}$$

  where the vector $\mathbf{s}(x,\omega) = \left\{s_j(x,\omega)\right\}^T, \forall\, j = 1,2$ and the complex matrix $\mathbf{\Gamma}(\omega) \in \mathbb{C}^{2\times 2}$ depends on the boundary conditions.
- In order to obtain $\mathbf{s}(x,\omega)$ first assume that

$$u(x) = \bar{u}\exp\left[kx\right] \tag{29}$$

  where k is the wave number. Substituting this in Eq. (5) we have

$$k^2 + \alpha^2 = 0 \quad \text{or} \quad k = \pm \mathrm{i}\alpha \tag{30}$$

Complex shape functions

- In view of the solutions in Eq. (30), the complex displacement field within the element can be expressed by a linear combination of the basis functions $e^{-\mathrm{i}\alpha x}$ and $e^{\mathrm{i}\alpha x}$ so that in our notations $\mathbf{s}(x,\omega) = \left\{e^{-\mathrm{i}\alpha x}, e^{\mathrm{i}\alpha x}\right\}^T$.
- Therefore, it is more convenient to express $\mathbf{s}(x,\omega)$ in terms of trigonometric functions. Considering $e^{\pm\mathrm{i}\alpha x} = \cos(\alpha x) \pm \mathrm{i}\sin(\alpha x)$, the vector $\mathbf{s}(x,\omega)$ can be alternatively expressed as

$$\mathbf{s}(x,\omega) = \begin{Bmatrix} \sin(\alpha x) \\ \cos(\alpha x) \end{Bmatrix} \in \mathbb{C}^2 \tag{31}$$

Complex shape functions

- Considering unit axial displacement boundary condition as $u_e(x = 0, \omega) = 1$ and $u_e(x = L, \omega) = 1$, after some elementary algebra, the shape function vector can be expressed in the form of Eq. (28) as

$$\mathbf{N}(x, \omega) = \mathbf{\Gamma}(\omega)\mathbf{s}(x, \omega), \quad \text{where} \quad \mathbf{\Gamma}(\omega) = \begin{bmatrix} -\cot(\alpha L) & 1 \\ \csc(\alpha L) & 0 \end{bmatrix} \in \mathbb{C}^{2\times 2} \tag{32}$$

- Simplifying this we obtain the dynamic shape functions as

$$\mathbf{N}(x, \omega) = \begin{bmatrix} -\cot(\alpha L)\sin(\alpha x) + \cos(\alpha x) \\ \csc(\alpha L)\sin(\alpha x) \end{bmatrix} \tag{33}$$

- Taking the limit as ω goes to 0 (that is the static case) it can be shown that the shape function matrix in Eq. (33) reduces to the classical shape function matrix given by Eq. (24). Therefore the shape functions given by Eq. (33) can be viewed as the generalisation of the nonlocal dynamical case.

Dynamic stiffness matrix

- The stiffness and mass matrices can be obtained similarly to the static finite element case discussed before.
- Note that for this case all the matrices become complex and frequency-dependent.
- It is more convenient to define the dynamic stiffness matrix as

$$\mathbf{D}_e(\omega) = \mathbf{K}_e(\omega) - \omega^2 \mathbf{M}_e(\omega) \tag{34}$$

so that the equation of dynamic equilibrium is

$$\mathbf{D}_e(\omega)\widehat{\mathbf{u}}_e(\omega) = \widehat{\mathbf{f}}(\omega) \tag{35}$$

- In Eq. (34), the frequency-dependent stiffness and mass matrices can be obtained as

$$\mathbf{K}_e(\omega) = EA \int_0^L \frac{d\mathbf{N}(x,\omega)}{dx} \frac{d\mathbf{N}^T(x,\omega)}{dx} \mathrm{d}x$$

$$\text{and} \quad \mathbf{M}_e(\omega) = m \int_0^L \mathbf{N}(x,\omega)\mathbf{N}^T(x,\omega) \mathrm{d}x \tag{36}$$

Dynamic stiffness matrix

- After some algebraic simplifications [19, 31] it can be shown that the dynamic stiffness matrix is given by the following closed-form expression

$$\mathbf{D}_e(\omega) = EA\alpha \begin{bmatrix} \cot(\alpha L) & -\csc(\alpha L) \\ \csc(\alpha L) & \cot(\alpha L) \end{bmatrix} \tag{37}$$

- This is in general a 2×2 matrix with complex entries. The frequency response of the system at the nodal point can be obtained by simply solving Eq. (35) for all frequency values.
- The calculation only involves inverting a 2×2 complex matrix and the results are exact with only one element for any frequency value.
- This is a significant advantage of the proposed dynamic finite element approach compared to the conventional finite element approach discussed in the pervious subsection.

Nodal forces

- A distributed body force can be considered following the usual finite element approach [29] and replacing the static shape functions with the dynamic shape functions (33).
- Suppose $p_e(x,\omega), x \in [0, L]$ is the frequency depended distributed body force. The element nodal forcing vector can be obtained as

$$\mathbf{f}_e(\omega) = \int_0^L p_e(x,\omega)\mathbf{N}(x,\omega)\mathrm{d}x \tag{38}$$

- As an example, if a point harmonic force of magnitude p is applied at length $b < L$ then, $p_e(x,\omega) = p\delta(x-b)$ where $\delta(\bullet)$ is the Dirac delta function.
- The element nodal force vector becomes

$$\mathbf{f}_e(\omega) = p\int_0^L \delta(x-b)\mathbf{N}(x,\omega)\mathrm{d}x = p\left\{\begin{array}{c} -\cot(\alpha L)\sin(\alpha b) + \cos(\alpha b) \\ \csc(\alpha L)\sin(\alpha b) \end{array}\right\} \tag{39}$$

Numerical example

- We consider only mass proportional damping such that the damping factor $\zeta_2 = 0.05$ and $\zeta_1 = 0$.
- A range of values of $e_0 a$ within 0-2 nm are used to understand its role in the dynamic response.
- Although the role of the nonlocal parameter on the natural frequencies has been investigated, its effect on the dynamic response is relatively unknown.
- It is assumed that the SWCNT is fixed at one end and we are interested in the frequency response at the free end due to harmonic excitation.
- Using the dynamic finite element approach only one 'finite element' is necessary as the equation of motion is solved exactly.
- We consider dynamic response of the CNT due to a harmonic force at the free edge.

Shape function $N_1(x,\omega)$ for $e_0a = 0.5$ nm

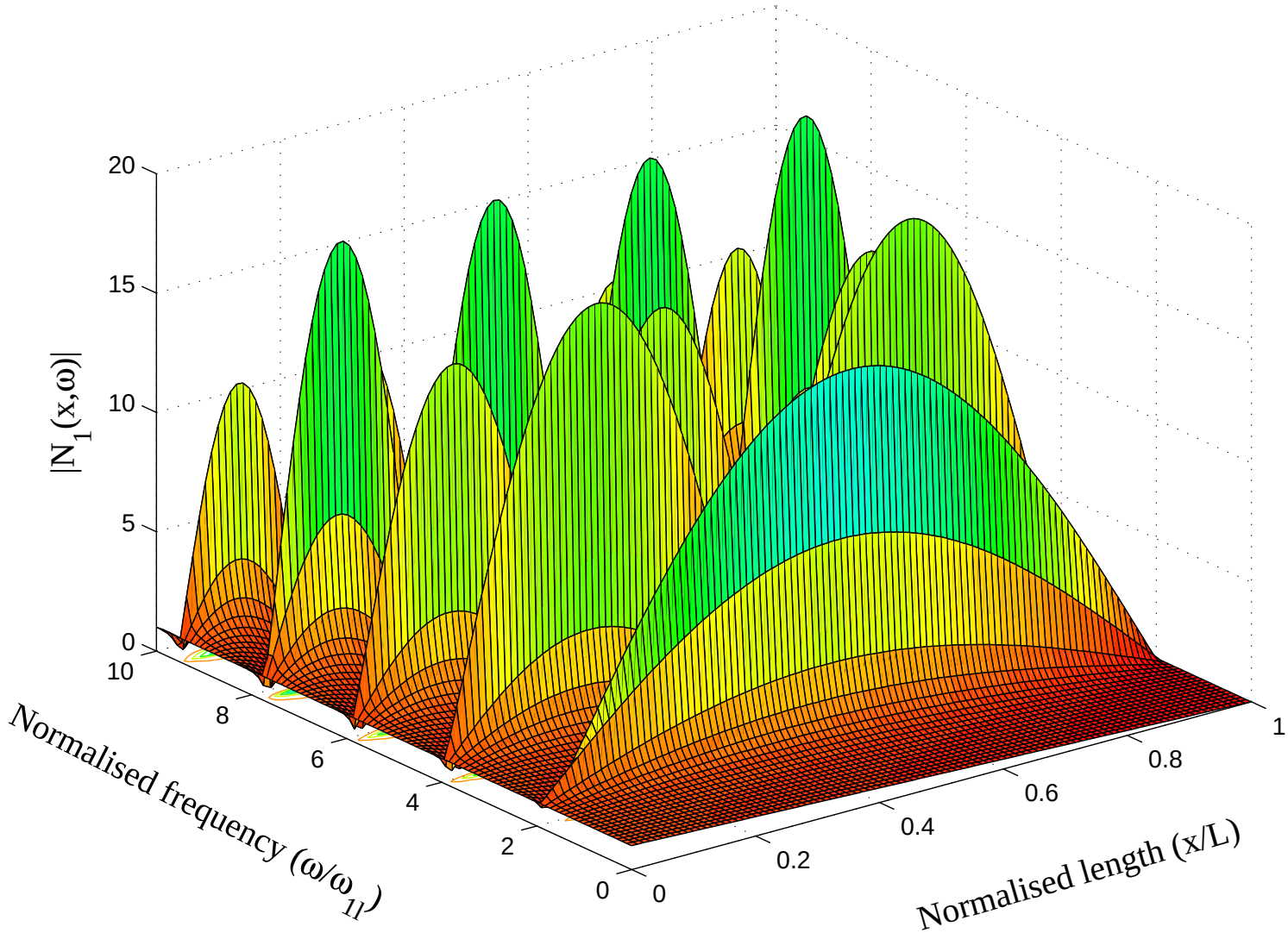

Amplitude of the shape function $N_1(x,\omega)$ with normalised frequency axes.

Shape function $N_2(x,\omega)$ for $e_0a = 0.5$ nm

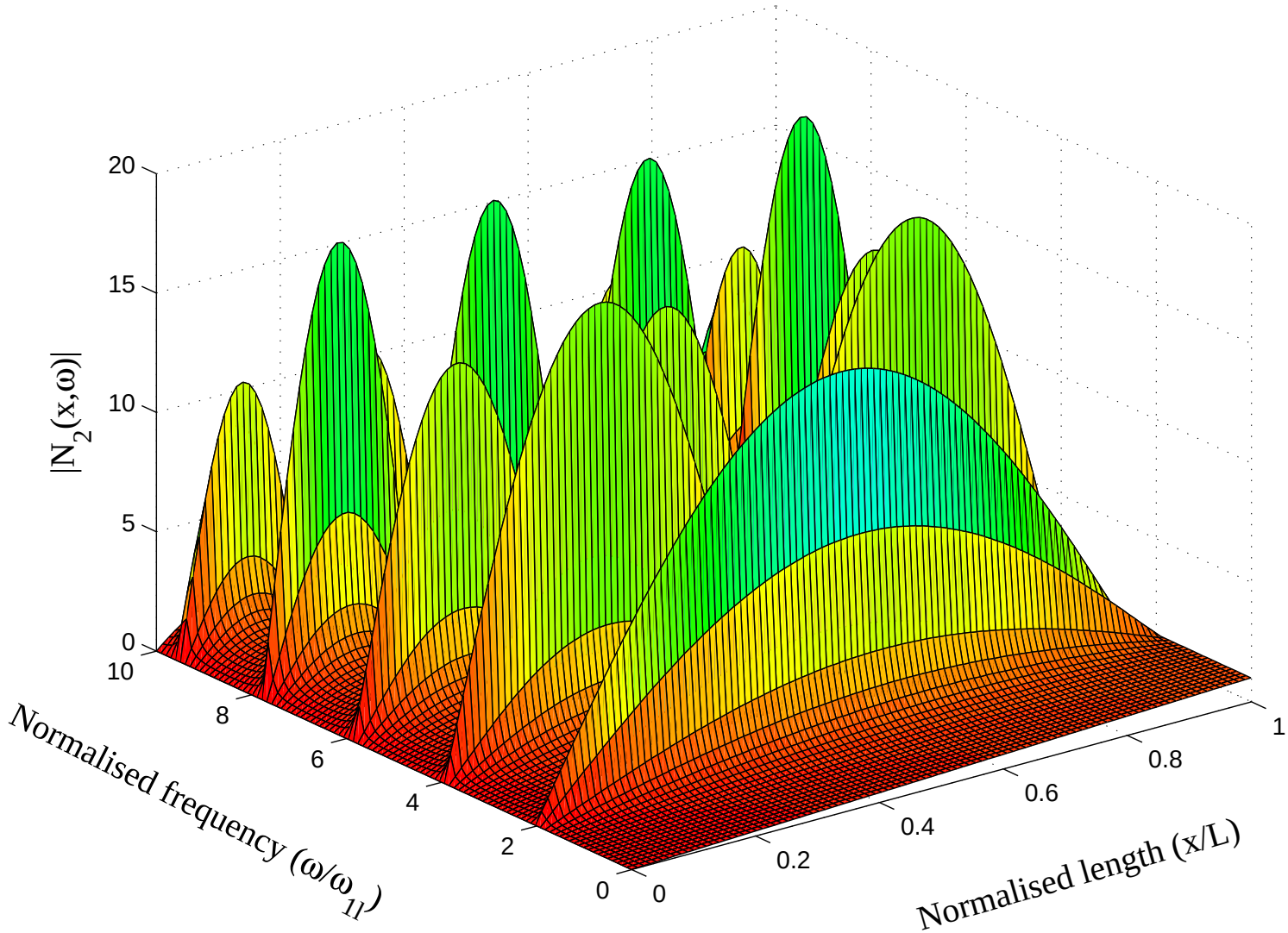

Amplitude of the shape function $N_2(x,\omega)$ with normalised frequency axes.

Dynamic shape functions

- The amplitudes of the two dynamic shape functions as a function of frequency for $e_0 a = 0.5$ nm are shown.
- For convenience, the shape functions are plotted against normalised frequency

$$\widehat{\omega} = \omega / \omega_{1l} \tag{40}$$

  and normalised length coordinate x/L.
- Here ω_{1l} is the first natural frequency of the local rod [27], given by

$$\omega_{1l} = \frac{\pi}{2L}\sqrt{\frac{EA}{m}} \tag{41}$$

- The amplitudes of the two dynamic shape functions as a function of frequency for $e_0 a = 2.0$ nm are shown next to examine the influence of the nonlocal parameter on the dynamic shape functions.

Shape function $N_1(x,\omega)$ for $e_0a = 2.0$ nm

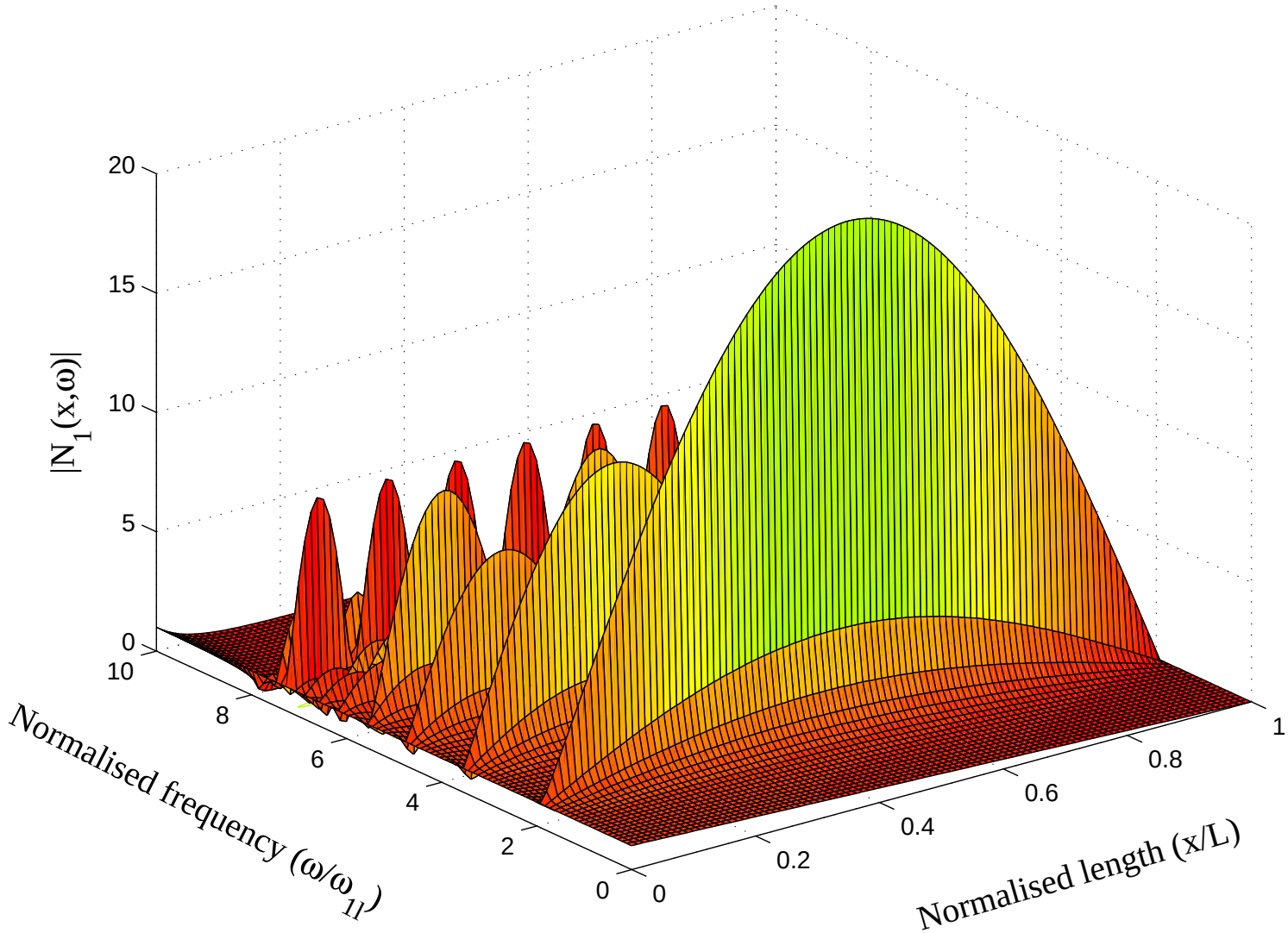

Amplitude of the shape function $N_1(x,\omega)$ with normalised frequency axes.

Shape function $N_2(x,\omega)$ for $e_0a = 2.0$ nm

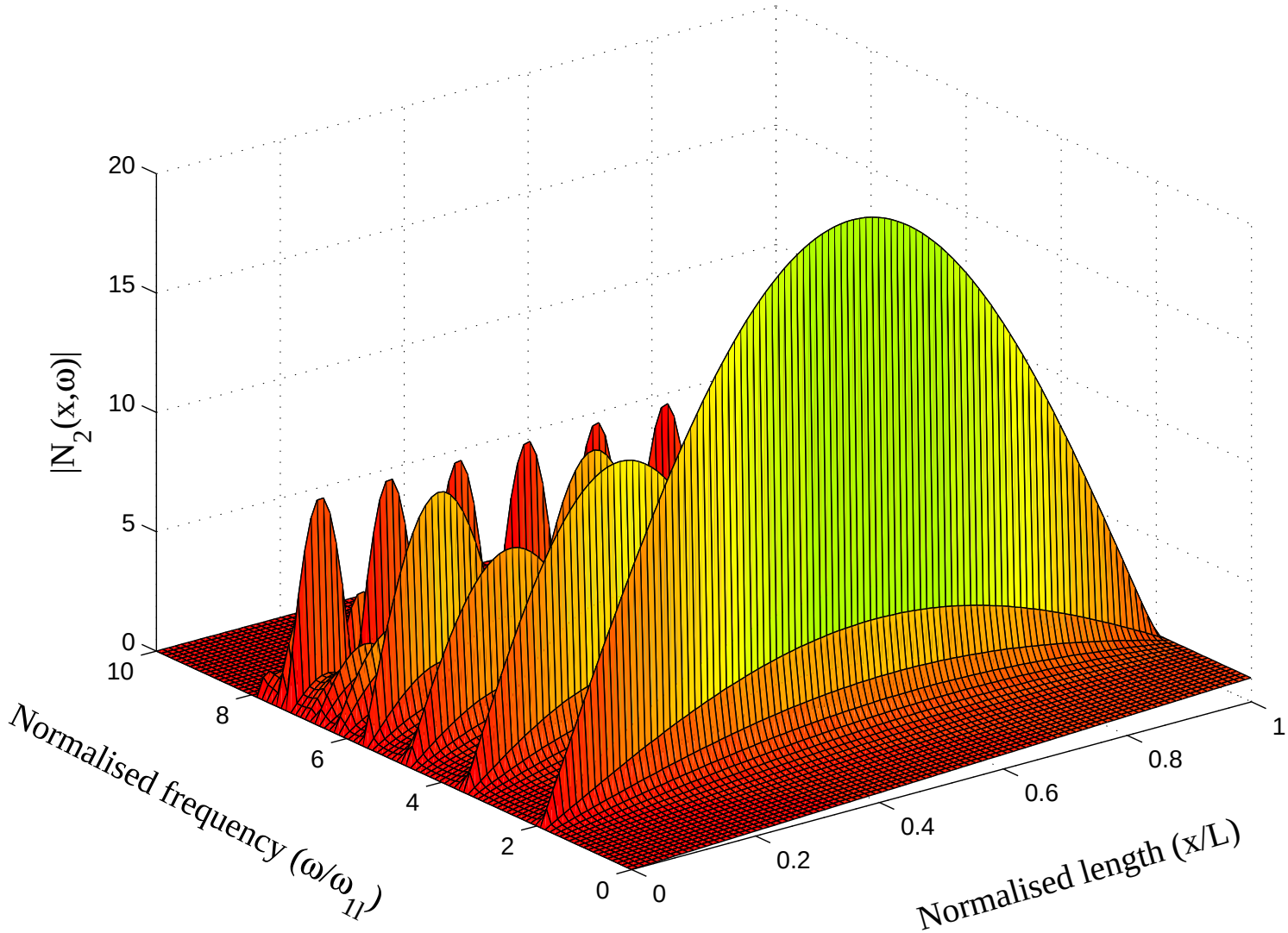

Amplitude of the shape function $N_2(x,\omega)$ with normalised frequency axes.

Dynamic shape functions

The plots of the shape functions show the following interesting features:

1. At zero frequency (that is for the static case) the shape functions reduce to the classical linear functions given by Eq. (24). It can be observed that $N_1(0,0) = 1$, $N_2(L,0) = 0$ and $N_2(0,0) = 0$, $N_2(L,0) = 1$.
2. For increasing frequency, the shape functions become nonlinear in x and adapt themselves according to the vibration modes. One can observe multiple modes in the higher frequency range. This nonlinearity in the shape functions is the key for obtaining the exact dynamic response using the proposed approach.
3. The figures also show the role of the nonlocal parameter. For the case of $e_0 a = 2.0$ nm one can observe more number of modes in the high frequency range. This is due to the fact that natural frequency of the nonlocal rod reduced with the increase in the value of the nonlocal parameter.

Frequency response

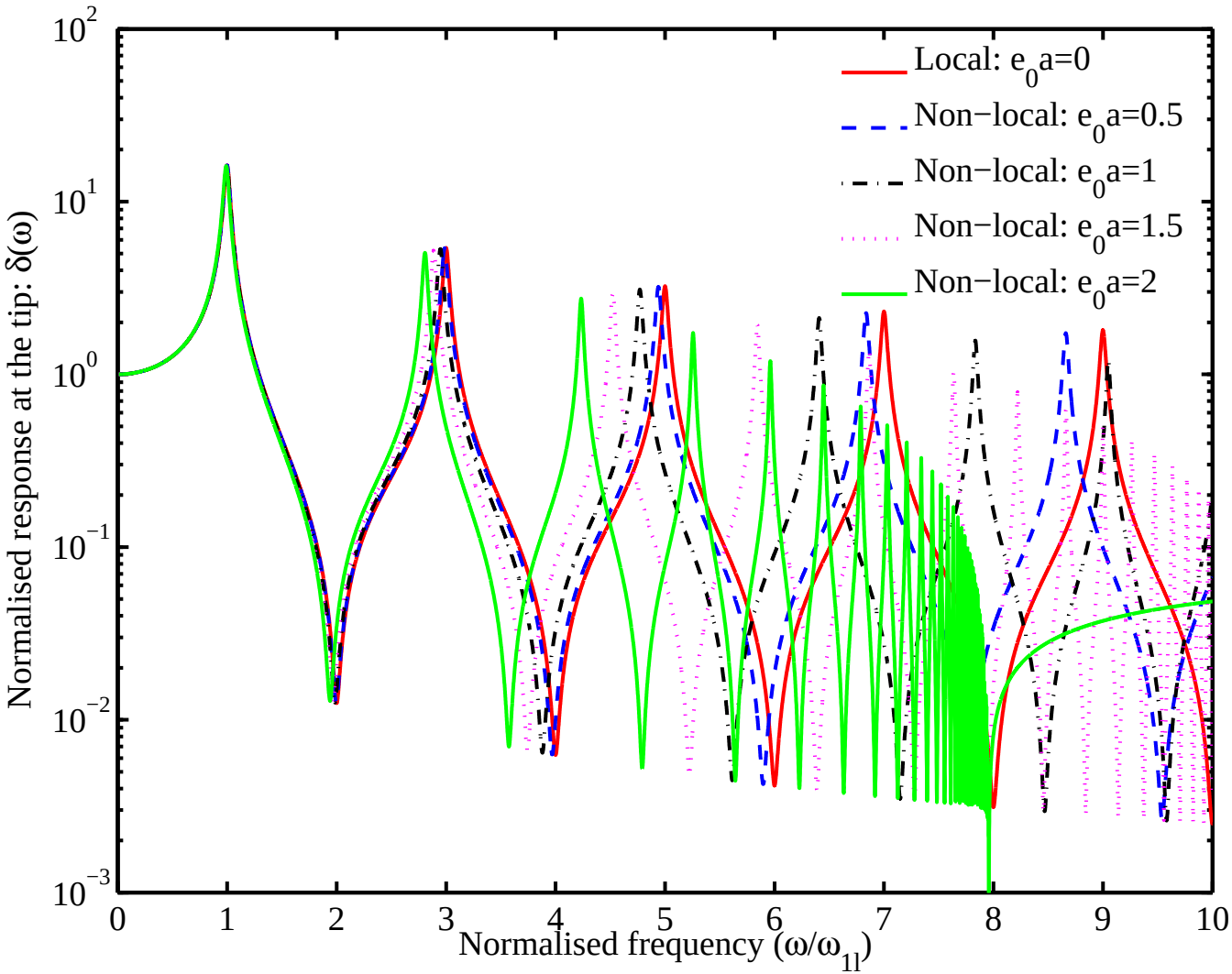

Normalised dynamic frequency response amplitude.

Frequency response

- The normalised displacement amplitude is defined by

$$\delta(\omega) = \frac{\widehat{u}_2(\omega)}{u_{\text{static}}} \tag{42}$$

where u_{static} is the static response at the free edge given by $u_{\text{static}} = FL/EA$.

- Assuming the amplitude of the harmonic excitation at the free edge is F, the dynamic response can be obtained using the equation of dynamic equilibrium (35) as

$$\widehat{u}_2(\omega) = \frac{F}{EA\alpha\cot(\alpha L)} = \frac{F\tan(\alpha L)}{EA\alpha} \tag{43}$$

- Therefore, the normalised displacement amplitude in Eq. (42) is given by

$$\delta(\omega) = \frac{\widehat{u}_2(\omega)}{u_{\text{static}}} = \left(\frac{F\tan(\alpha L)}{EA\alpha}\right)/(FL/EA) = \frac{\tan(\alpha L)}{\alpha L} \tag{44}$$

- The frequency axis of the response amplitude is normalised similarly to the plots of the shape functions given earlier.

Frequency response

- The consequence of the asymptotic upper limit can be seen in the frequency response amplitude plot.
- For higher values $e_0 a$, more and more resonance peaks are clustered within a frequency band.
- Indeed in Eq. (23) we have proved that asymptotically, the spacing between the natural frequencies goes to zero. This implies that higher natural frequencies of a nonlocal system are very closely spaced.
- This fact can be observed in the frequency band $7 \lesssim \widehat{\omega} \lesssim 8$ for the case when $e_0 a = 2$ nm. The same behaviour is expected for other values of $e_0 a$ in the higher frequency ranges.
- It is worth pointing out that the frequency response curve for the case of $e_0 a = 2.0$ nm is invalid after $\widehat{\omega} > 8$ as it is beyond the maximum frequency limit.
- It can also be seen that the resonance peak shifts to the left for increasing values of $e_0 a$. This shift corresponds to the reduction in the natural frequencies as shown in before.

Dynamic vs. conventional FEM

- We compare the results from the dynamic finite element and conventional finite element methods.
- The natural frequencies can be obtained using the conventional nonlocal finite element method.
- By assembling the element stiffness and mass matrices given by Eqs. (25) and (26) and solving the resulting matrix eigenvalue problem $\mathbf{K}\phi_j = \omega_j^2 \mathbf{M}\phi_j, j = 1, 2, \cdots$ one can obtain the both the eigenvalues and eigenvectors (denoted by ϕ_j here).
- For the numerical calculation we used 100 elements. This in turn, results in global mass and stiffness matrices of dimension 200×200.

Dynamic vs. conventional FEM

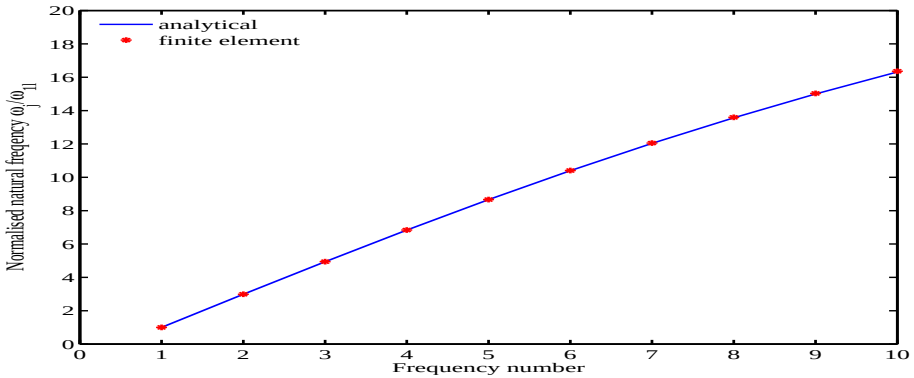

(a) $e_0a = 0.5$nm

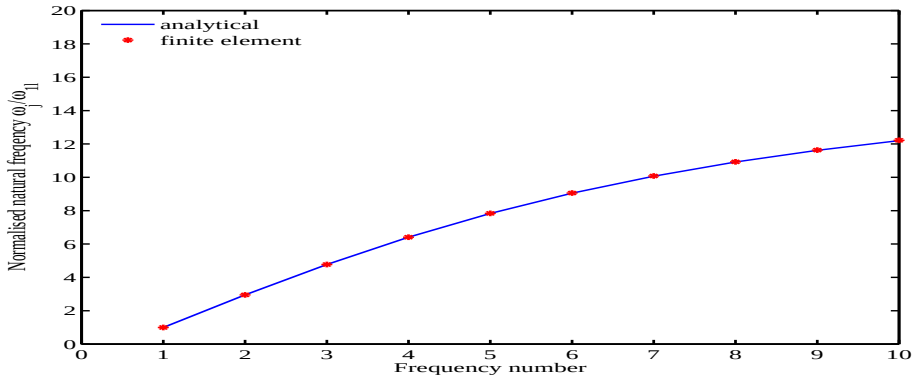

(b) $e_0a = 1.0$nm

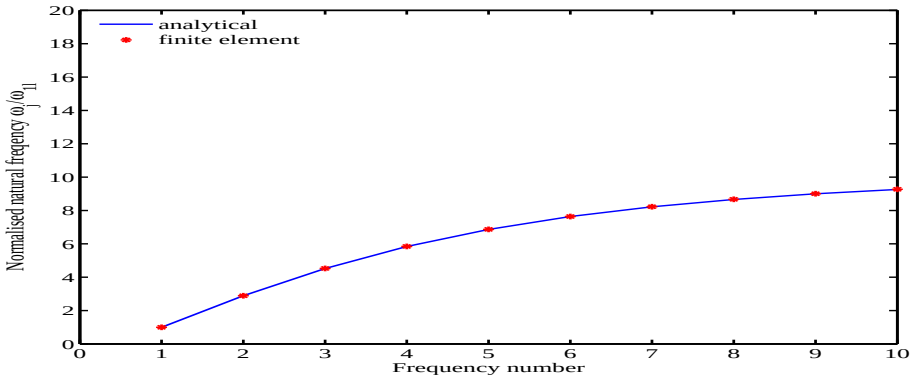

(c) $e_0a = 1.5$nm

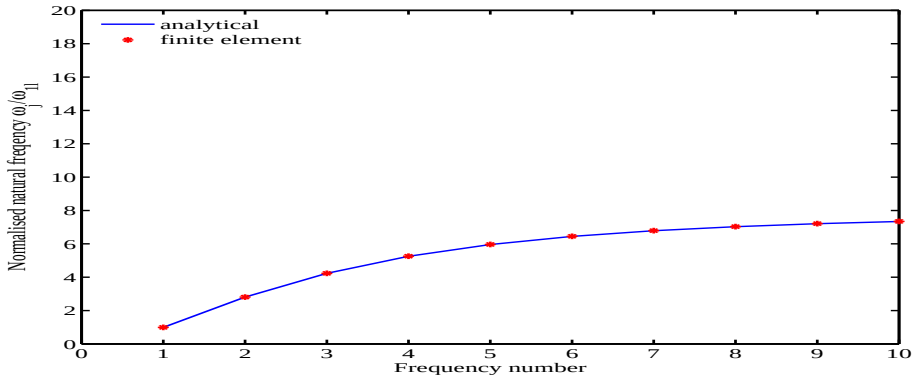

(d) $e_0a = 2.0$nm

Figure: Normalised natural frequency (ω_j/ω_{1l}) at the tip for different values of e_0a. Analytical results are compared with the finite element (with 100 elements) results.

Dynamic vs. conventional FEM

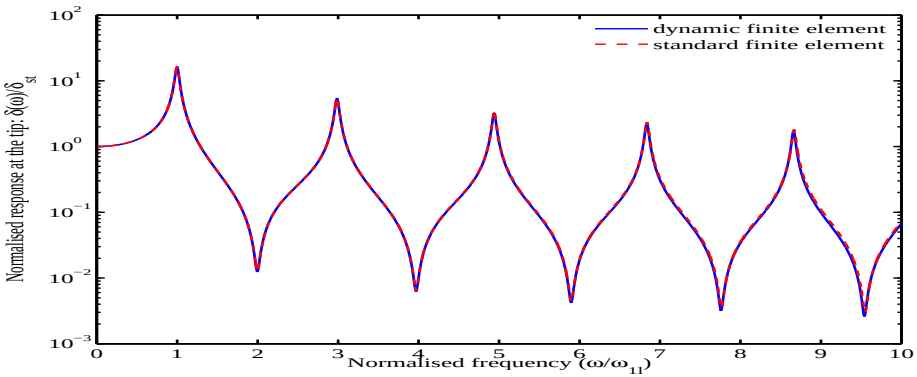

(a) $e_0 a = 0.5$nm

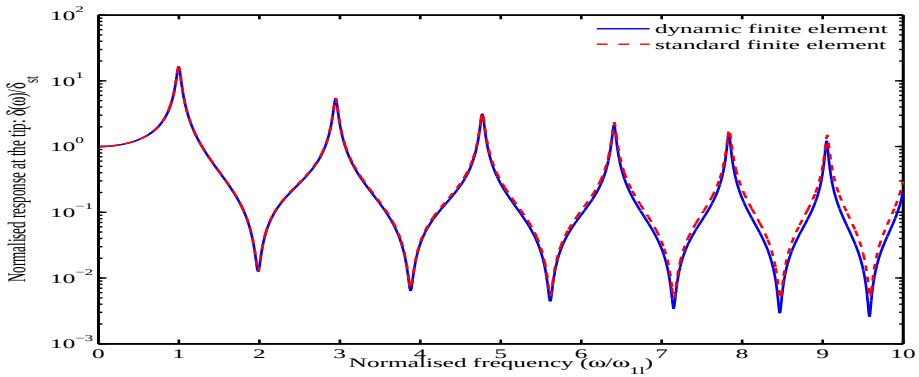

(b) $e_0 a = 1.0$nm

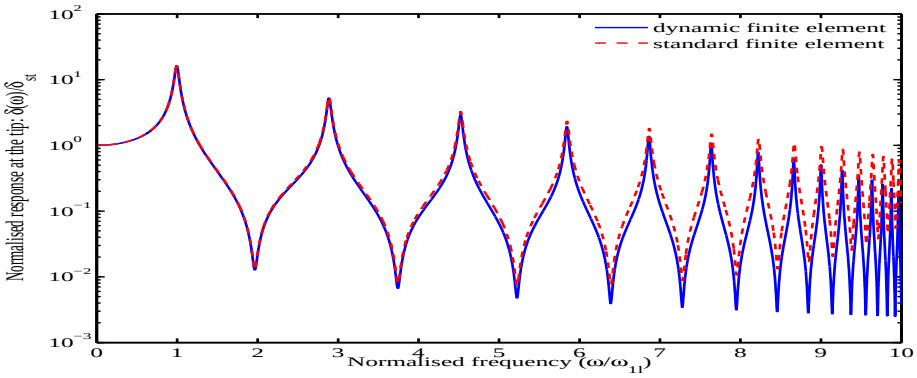

(c) $e_0 a = 1.5$nm

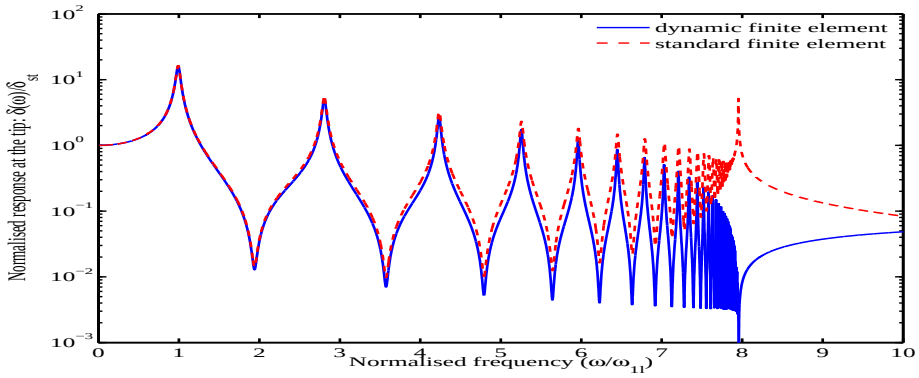

(d) $e_0 a = 2.0$nm

Figure: Amplitude of the normalised dynamic frequency response at the tip for different values of $e_0 a$. Dynamic finite element results (with one element) is compared with the conventional finite element results (with 100 elements).

Dynamic vs. conventional FEM

- Excellent agreement was found for the first 10 natural frequencies.
- However, the results become quite different for the dynamic response.
- In the numerical calculations, 10^5 points are used in the frequency axis. The frequency response functions from the standard finite element were obtained using the classical modal series method [27].
- For small values of $e_0 a$ the results from the dynamic finite element and standard finite element method agree well, as seen in (a) and (b).
- The discrepancies between the methods increase for higher values of $e_0 a$ as seen in (c) and (d).

Dynamic vs. conventional FEM

- The results from the dynamic finite element approach are exact as it does not suffer from error arising due to finite element discretisation.
- For higher values of $e_0 a$, increasing numbers of natural frequencies lie within a given frequency range. As a result a very fine mesh is necessary to capture the high number of modes.
- If the given frequency is close the the maximum cutoff frequency, then a very high number of finite elements will be necessary (theoretically infinitely many and there exist an infinite number of frequencies upto the cut off frequency).
- In such a situation effectively the conventional finite element analysis breaks down, as seen in (d) in the range $7 \leq \widehat{\omega} < 8$. The proposed dynamic finite element is effective in these situations as it does not suffer from discretisation errors as in the conventional finite element method.

Summary

- Strain rate dependent viscous damping and velocity dependent viscous damping are considered.
- Damped and undamped natural frequencies for general boundary conditions are derived.
- An asymptotic analysis is used to understand the behaviour of the frequencies and their spacings in the high-frequency limit.
- Frequency dependent complex-valued shape functions are used to obtain the dynamic stiffness matrix in closed form.
- The dynamic response in the frequency domain can be obtained by inverting the dynamic stiffness matrix.
- The stiffness and mass matrices of the nonlocal rod were also obtained using the conventional finite element method. In the special case when the nonlocal parameter becomes zero, the expression of the mass matrix reduces to the classical case.
- The proposed method is numerically applied to the axial vibration of a (5,5) carbon nanotube.

Main results

- Unlike local rods, nonlocal rods have an upper cut-off natural frequency. Using an asymptotic analysis, it was shown that for an undamped rod, the natural frequency $(\omega_{k_{\max}}) \to \frac{1}{(e_0 a)}\sqrt{\frac{EA}{m}}$. This maximum frequency does not depend on the boundary conditions or the length of the rod.
- Near to the maximum frequency, the spacing between the natural frequencies becomes very small. This in turn leads to clustering of the resonance peaks near the maximum frequency.
- For the oscillation frequency of damped systems, the upper cut-off frequency is given by $(\omega_{k_{\max}}) \to \frac{c}{(e_0 a)}\sqrt{1-\left(\frac{\zeta_1 c}{2e_0 a}\right)^2}$ where $c = \sqrt{EA/m}$ and ζ_1 is the stiffness proportional damping factor arising from the strain rate dependent viscous damping constant. The velocity dependent viscous damping has no affect on the maximum frequency of the damped rod.
- The asymptotic critical damping factor for nonlocal rods is given by $(\zeta_1)_{\text{crit}} = 2e_0 a\sqrt{\frac{m}{EA}}$.

Nano mechanical sensors

- Progress in nanotechnologies has brought about a number of highly sensitive label-free biosensors.
- These include electronic biosensors based on nanowires and nanotubes, optical biosensors based on nanoparticles and mechanical biosensors based on resonant micro- and nanomechanical suspended structures.
- In these devices, molecular receptors such as antibodies or short DNA molecules are immobilized on the surface of the micro-nanostructures. The operation principle is that molecular recognition between the targeted molecules present in a sample solution and the sensor-anchored receptors gives rise to a change of the optical, electrical or mechanical properties depending on the class of sensor used.
- These sensors can be arranged in dense arrays by using established micro- and nanofabrication tools.

Cantilever nano-sensor

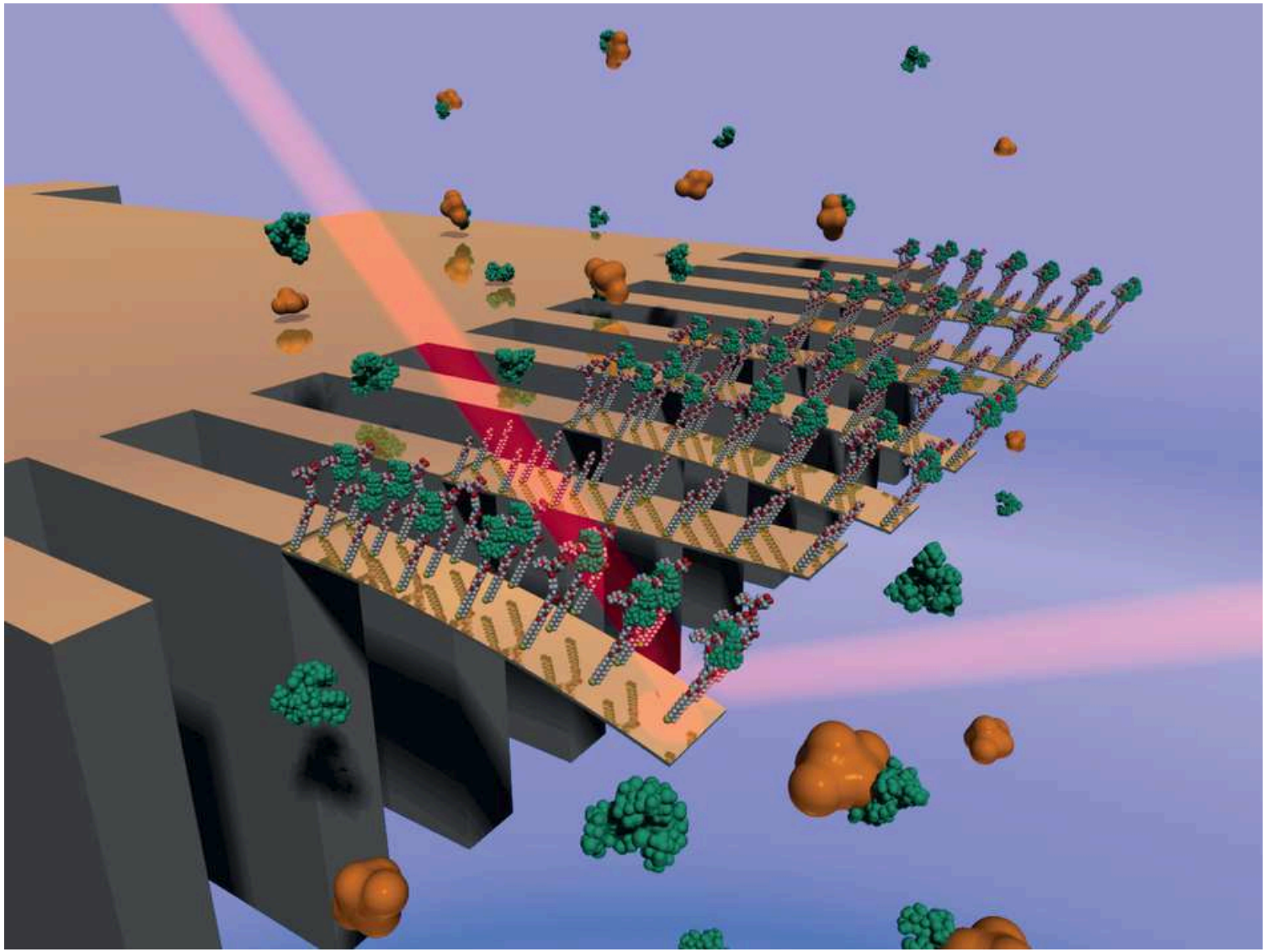

Array of cantilever nano sensors (from http://www.bio-nano-consulting.com)

Cantilever nano-sensor

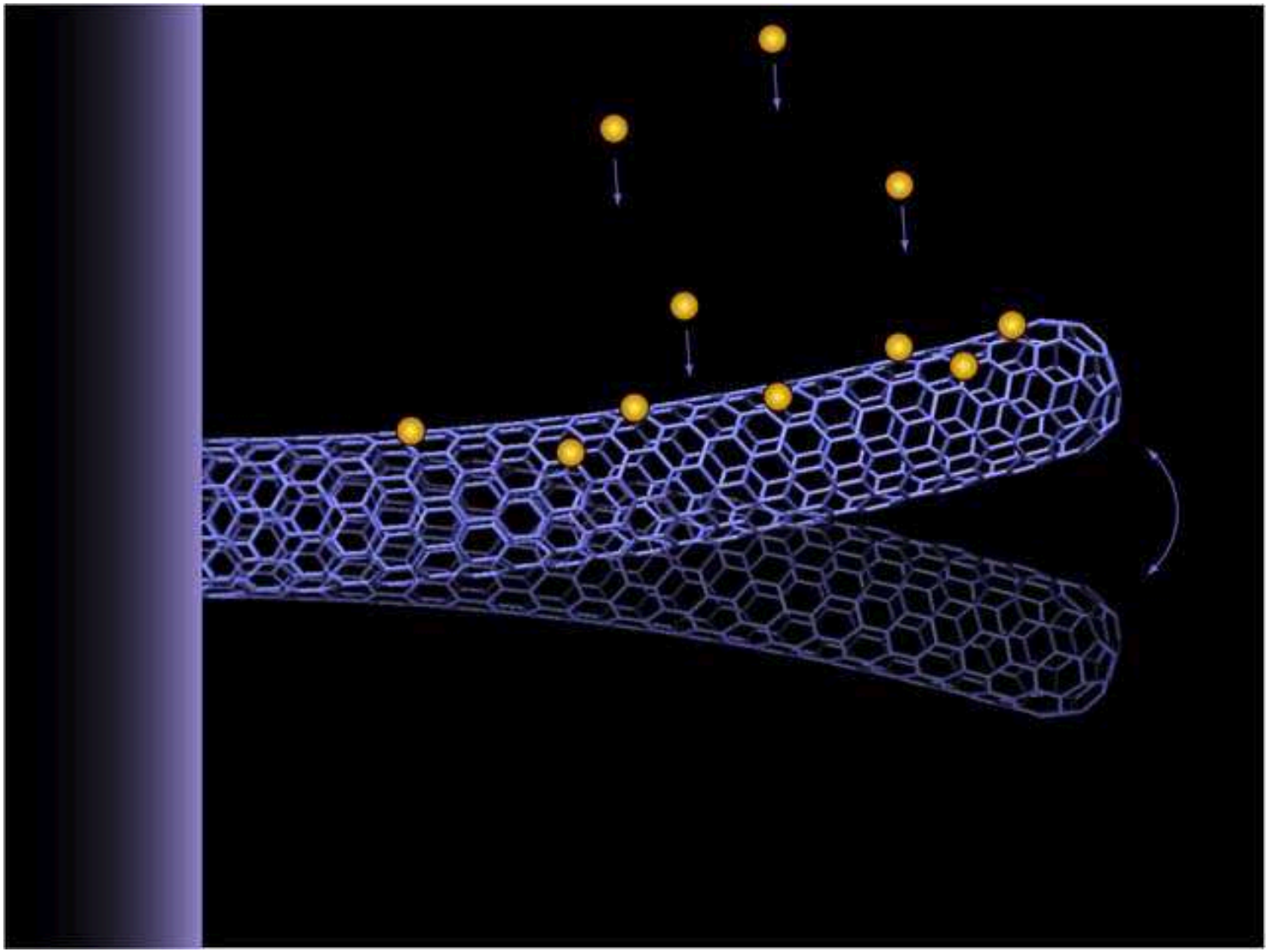

Carbon nanotube with attached molecules

The mechanics behind nano-sensors

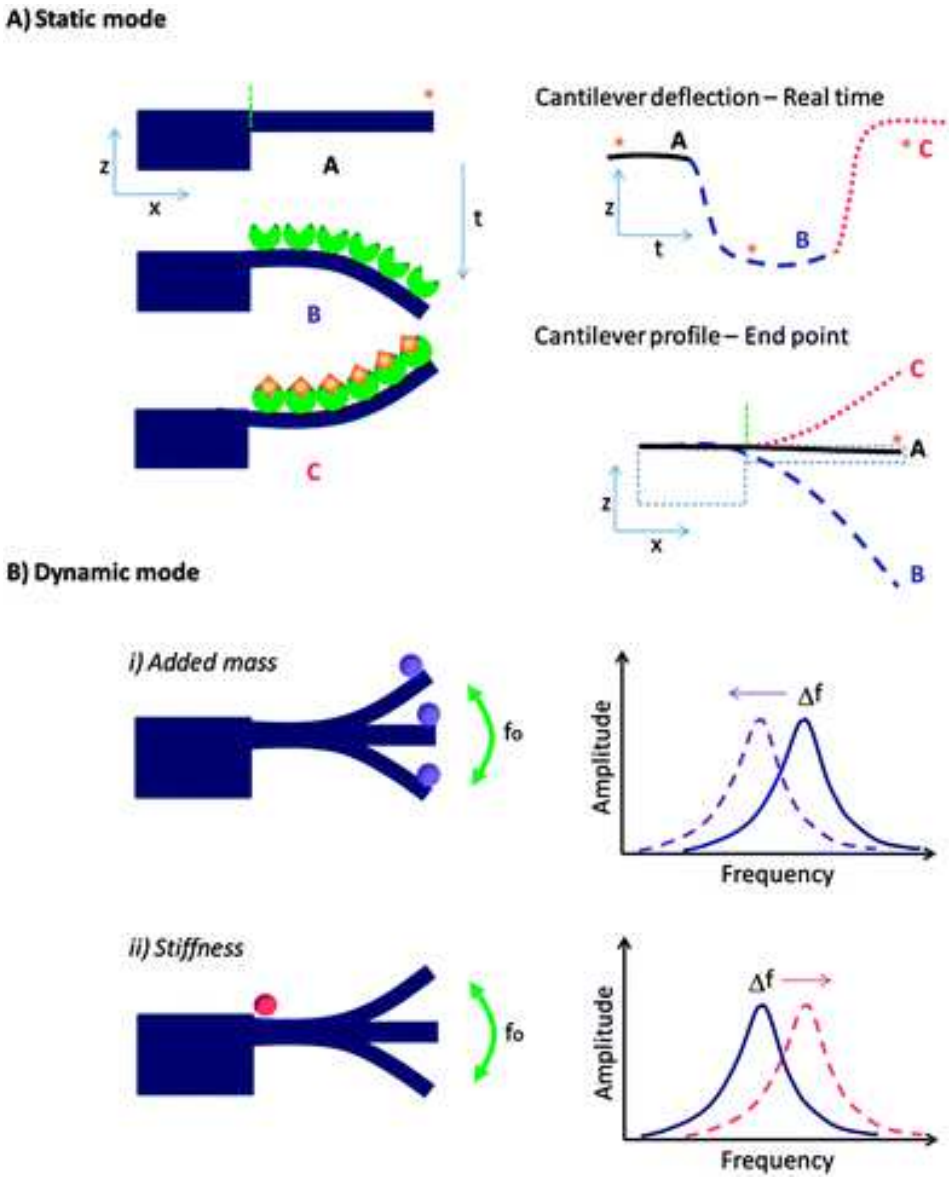

Mass sensing - an inverse problem

- This talk will focus on the detection of mass based on shift in frequency.
- Mass sensing is an inverse problem.
- The "answer" in general in non-unique. An added mass at a certain point on the sensor will produce an unique frequency shift. However, for a given frequency shift, there can be many possible combinations of mass values and locations.
- Therefore, predicting the frequency shift - the so called "forward problem" is not enough for sensor development.
- Advanced modelling and computation methods are available for the forward problem. However, they may not be always readily suitable for the inverse problem if the formulation is "complex" to start with.
- Often, a carefully formulated simplified computational approach could be more suitable for the inverse problem and consequently for reliable sensing.

The need for “instant” calculation

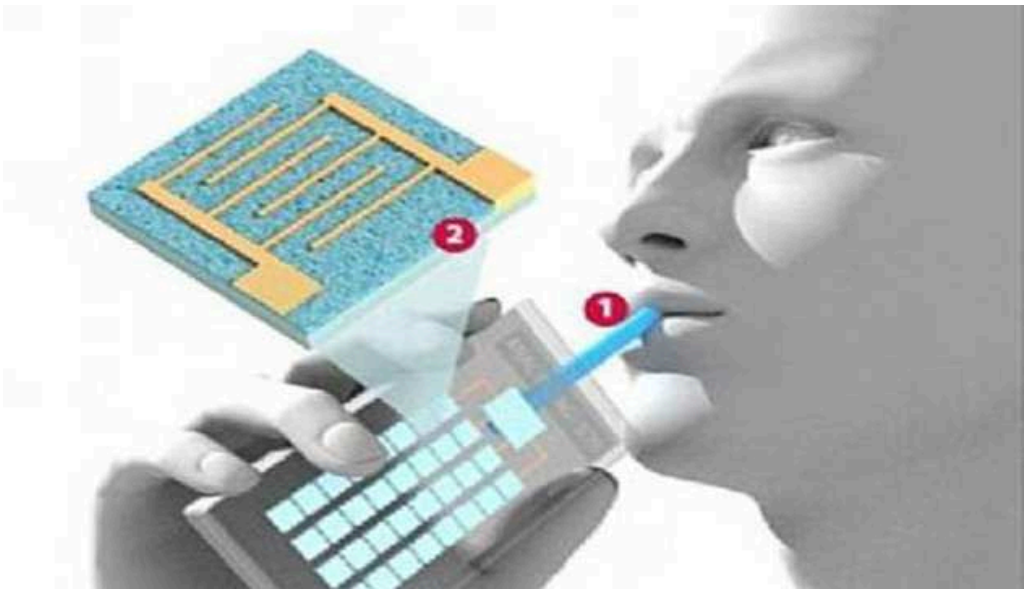

Sensing calculations must be performed very quickly - almost in real time with very little computational power (fast and cheap devices).

Single-walled carbon nanotube based sensors

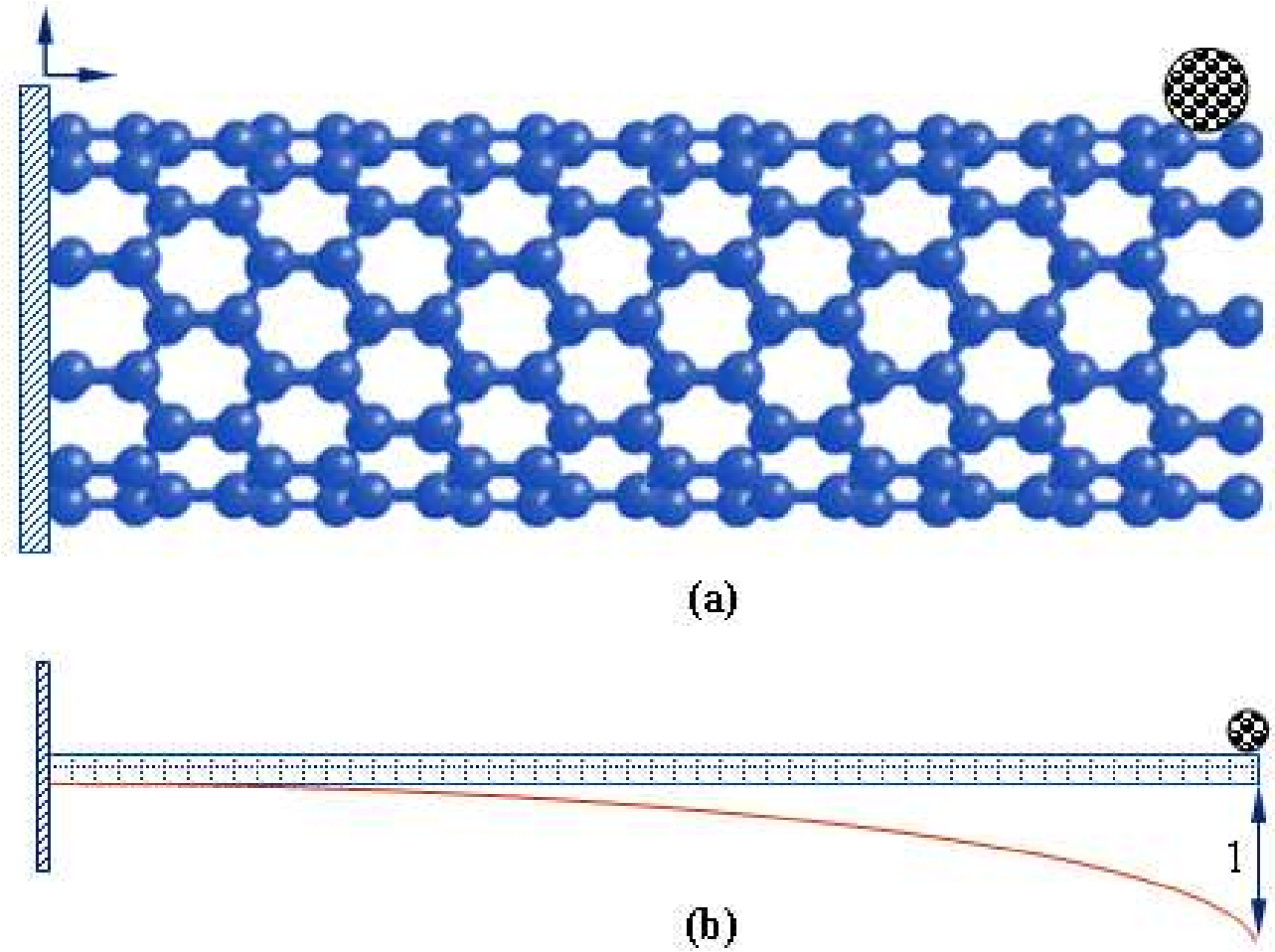

Cantilevered nanotube resonator with an attached mass at the tip of nanotube length: (a) Original configuration; (b) Mathematical idealization. Unit deflection under the mass is considered for the calculation of kinetic energy of the nanotube.

Single-walled carbon nanotube based sensors - bridged case

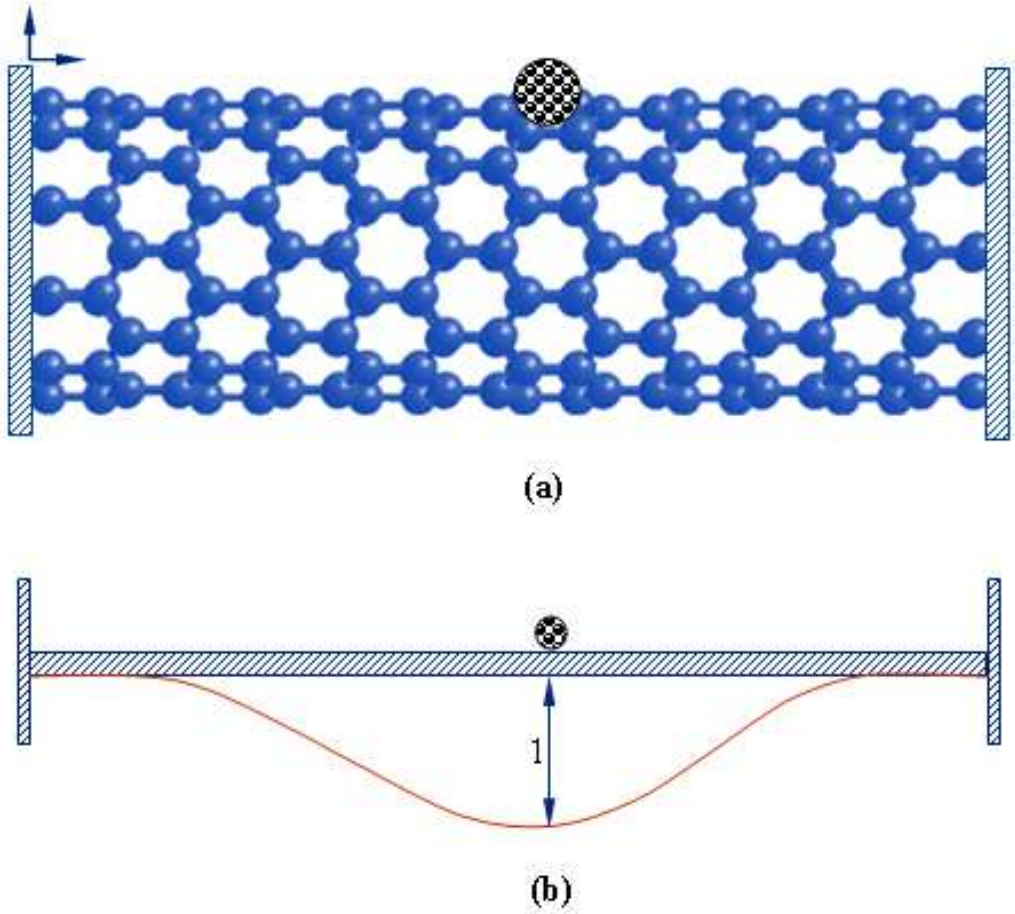

Bridged nanotube resonator with an attached mass at the center of nanotube length: (a) Original configuration; (b) Mathematical idealization. Unit deflection under the mass is considered for the calculation of kinetic energy of the nanotube.

Resonant frequencies of SWCNT with attached mass

- In order to obtain simple analytical expressions of the mass of attached biochemical entities, we model a single walled CNT using a uniform beam based on classical Euler-Bernoulli beam theory:

$$EI\frac{\partial^4 y(x,t)}{\partial x^4} + \rho A\frac{\partial^2 y(x,t)}{\partial t^2} = 0 \tag{45}$$

where E the Youngs modulus, I the second moment of the cross-sectional area A, and ρ is the density of the material. Suppose the length of the SWCNT is L.

- Depending on the boundary condition of the SWCNT and the location of the attached mass, the resonant frequency of the combined system can be derived. We only consider the fundamental resonant frequency, which can be expresses as

$$f_n = \frac{1}{2\pi}\sqrt{\frac{k_{eq}}{m_{eq}}} \tag{46}$$

Here k_{eq} and m_{eq} are respectively equivalent stiffness and mass of SWCNT with attached mass in the first mode of vibration.

Cantilevered SWCNT with mass at the tip

- Suppose the value of the added mass is M. We give a virtual force at the location of the mass so that the deflection under the mass becomes unity. For this case $F_{eq} = 3EI/L^3$ so that

$$k_{eq} = \frac{3EI}{L^3} \tag{47}$$

- The deflection shape along the length of the SWCNT for this case can be obtained as

$$Y(x) = \frac{x^2\,(3\,L - x)}{2L^3} \tag{48}$$

- Assuming harmonic motion, i.e., $y(x,t) = Y(x)\exp(i\omega t)$, where ω is the frequency, the kinetic energy of the SWCNT can be obtained as

$$\begin{aligned} T &= \frac{\omega^2}{2}\int_0^L \rho A Y^2(x)dx + \frac{\omega^2}{2}MY^2(L) \\ &= \rho A\frac{\omega^2}{2}\int_0^L Y^2(x)dx + \frac{\omega^2}{2}M\,1^2 = \frac{\omega^2}{2}\left(\frac{33}{140}\rho AL + M\right) \end{aligned} \tag{49}$$

Cantilevered SWCNT with mass at the tip

- Therefore

$$m_{eq} = \frac{33}{140}\rho AL + M \tag{50}$$

- The resonant frequency can be obtained using equation (66) as

$$\begin{aligned} f_n &= \frac{1}{2\pi}\sqrt{\frac{k_{eq}}{m_{eq}}} = \frac{1}{2\pi}\sqrt{\frac{3EI/L^3}{\frac{33}{140}\rho AL + M}} \\ &= \frac{1}{2\pi}\sqrt{\frac{140}{11}}\sqrt{\frac{EI}{\rho AL^4}}\sqrt{\frac{1}{1+\frac{M}{\rho AL}\frac{140}{33}}} = \frac{1}{2\pi}\frac{\alpha^2\beta}{\sqrt{1+\Delta M}} \end{aligned} \tag{51}$$

where

$$\alpha^2 = \sqrt{\frac{140}{11}} \quad \text{or} \quad \alpha = 1.888 \tag{52}$$

$$\beta = \sqrt{\frac{EI}{\rho AL^4}} \tag{53}$$

$$\text{and} \quad \Delta M = \frac{M}{\rho AL}\mu, \quad \mu = \frac{140}{33} \tag{54}$$

Cantilevered SWCNT with mass at the tip

- Clearly the resonant frequency for a cantilevered SWCNT with no added tip mass is obtained by substituting $\Delta M = 0$ in equation (51) as

$$f_{0_n} = \frac{1}{2\pi}\alpha^2\beta \tag{55}$$

- Combining equations (51) and (55) one obtains the relationship between the resonant frequencies as

$$f_n = \frac{f_{0_n}}{\sqrt{1+\Delta M}} \tag{56}$$

General derivation of the sensor equations

- The frequency-shift can be expressed using equation (56) as

$$\Delta f = f_{0_n} - f_n = f_{0_n} - \frac{f_{0_n}}{\sqrt{1 + \Delta M}} \tag{57}$$

- From this we obtain

$$\frac{\Delta f}{f_{0_n}} = 1 - \frac{1}{\sqrt{1 + \Delta M}} \tag{58}$$

- Rearranging gives the expression

$$\Delta M = \frac{1}{\left(1 - \frac{\Delta f}{f_{0_n}}\right)^2} - 1 \tag{59}$$

- This equation completely relates the change is mass frequency-shift. Expanding equation (59) is Taylor series one obtains

$$\Delta M = \sum_j (j+1) \left(\frac{\Delta f}{f_{0_n}}\right)^j, \quad j = 1, 2, 3, \ldots \tag{60}$$

General derivation of the sensor equations

- Therefore, keeping upto first and third order terms one obtains the linear and cubic approximations as

$$\Delta M \approx 2\left(\frac{\Delta f}{f_{0_n}}\right) \tag{61}$$

$$\text{and} \quad \Delta M \approx 2\left(\frac{\Delta f}{f_{0_n}}\right) + 3\left(\frac{\Delta f}{f_{0_n}}\right)^2 + 4\left(\frac{\Delta f}{f_{0_n}}\right)^3 \tag{62}$$

- The actual value of the added mass can be obtained from (59) as

Mass detection from frequency shift

$$M = \frac{\rho A L}{\mu}\frac{\left(\alpha^2\beta\right)^2}{\left(\alpha^2\beta - 2\pi\Delta f\right)^2} - \frac{\rho A L}{\mu} \tag{63}$$

- Using the linear approximation, the value of the added mass can be obtained as

$$M = \frac{\rho A L}{\mu}\frac{2\pi\Delta f}{\alpha^2\beta} \tag{64}$$

Comparison of sensing results

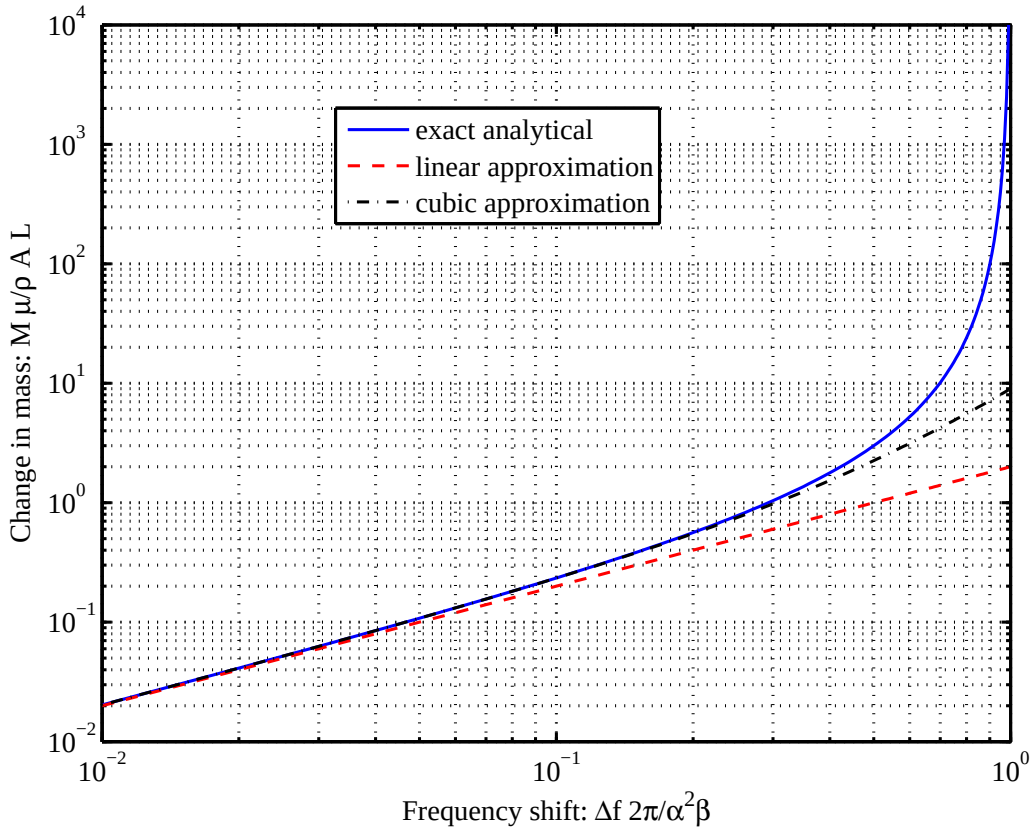

The general relationship between the normalized frequency-shift and normalized added mass of the bio-particles in a SWCNT with effective density ρ, cross-section area A and length L. Here $\beta = \sqrt{\frac{EI}{\rho AL^4}}\mathrm{s}^{-1}$, the nondimensional constant α depends on the boundary conditions and μ depends on the location of the mass. For a cantilevered SWCNT with a tip mass $\alpha^2 = \sqrt{140/11}$, $\mu = 140/33$ and for a bridged SWCNT with a mass at the midpoint $\alpha^2 = \sqrt{6720/13}$, $\mu = 35/13$.

Validation of sensor equations - FE model

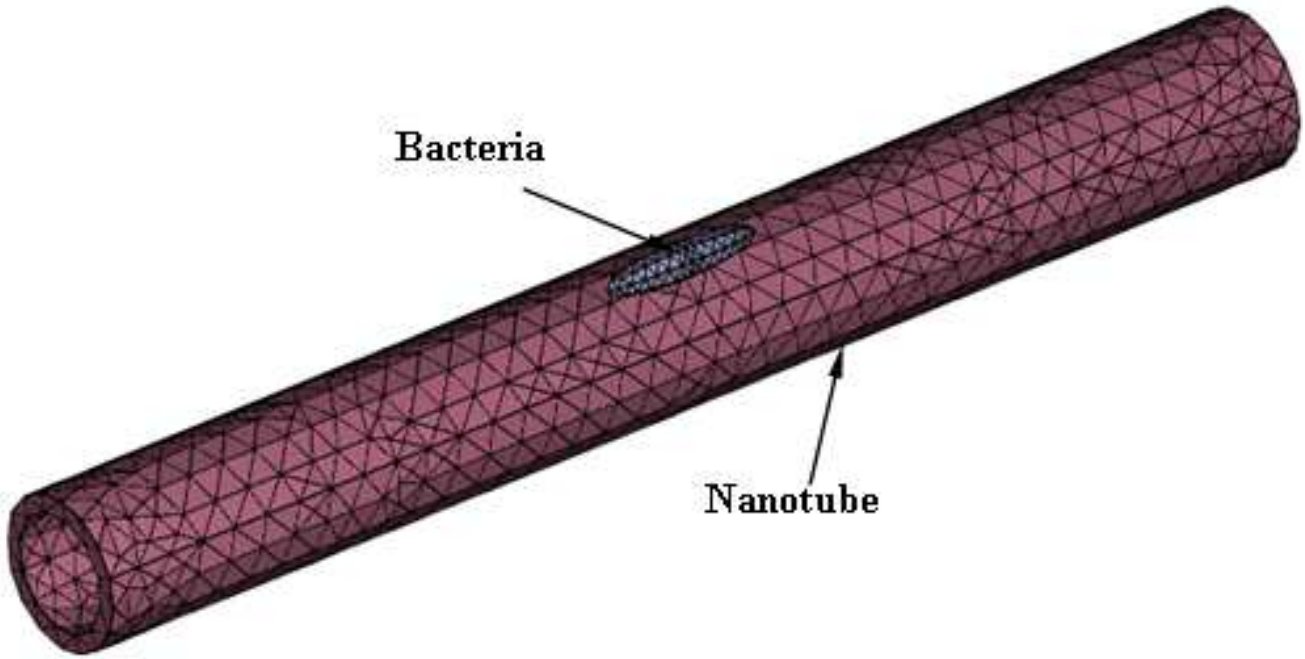

The theory of linear elasticity is used for both the CNT and the bacteria. FE model: number of degrees of freedom = 55401, number of mesh point = 2810, number of elements (tetrahedral element) = 10974, number of boundary elements (triangular element) = 3748, number of vertex elements = 22, number of edge elements = 432, minimum element quality = 0.2382 and element volume ratio = 0.0021. Length of the nanotube is 8 nm and length of bacteria is varied between 0.5 to 3.5 nm.

Validation of sensor equations - model data

Table: Geometrical and material properties for the single-walled carbon nanotube and the bacterial mass.

SWCNT	Bacteria (E Coli)
$L = 8$ nm	$E = 25.0MPa$
$E = 1.0TPa$	$\rho = 1.16g/cc$
$\rho = 2.24g/cc$	–
$D = 1.1nm$	–
$\nu = 0.30nm$	–

Validation of sensor equations - frequency values

Table: Comparison of frequencies (100 GHz) obtained from finite element simulation with MD simulation for the bridged configuration. For the 8.0 nm SWCNT used in this study, the maximum error is less than about 4%.

D(nm)	L(nm)		f_1	f_2	f_3	f_4	f_5
		MD	10.315	10.315	10.478	10.478	15.796
	4.1	*FE*	10.769	10.769	16.859	22.224	22.224
		%error	-4.40	-4.40	-60.90	-112.10	-40.69
		MD	6.616	6.616	9.143	9.143	11.763
1.1	5.6	*FE*	6.883	6.884	12.237	14.922	14.924
		%error	-4.04	-4.05	-33.84	-63.21	-26.87
		MD	3.800	3.8	8.679	8.679	8.801
	8.0	*FE*	3.900	3.9	8.659	9.034	9.034
		%error	-2.63	-2.63	-0.23	-4.09	-2.65

Validation of sensor equations - Cantilever nanotube

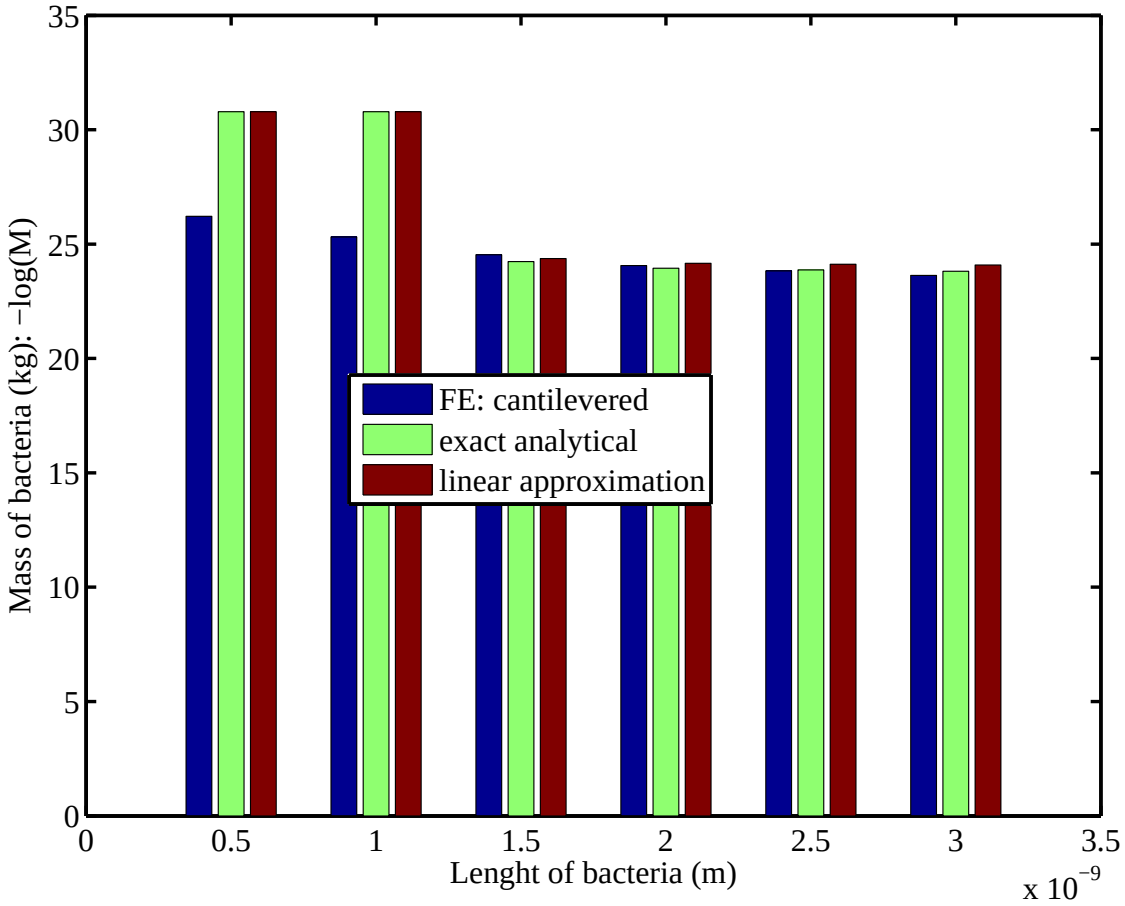

The variation of identified mass with bacterial length using the finite element simulation, exact analytical formula and the linear approximation for the cantilevered nanotube. Proposed analytical expressions are in good agreement with the detailed finite element results for longer bacterial length.

Validation of sensor equations - Bridged nanotube

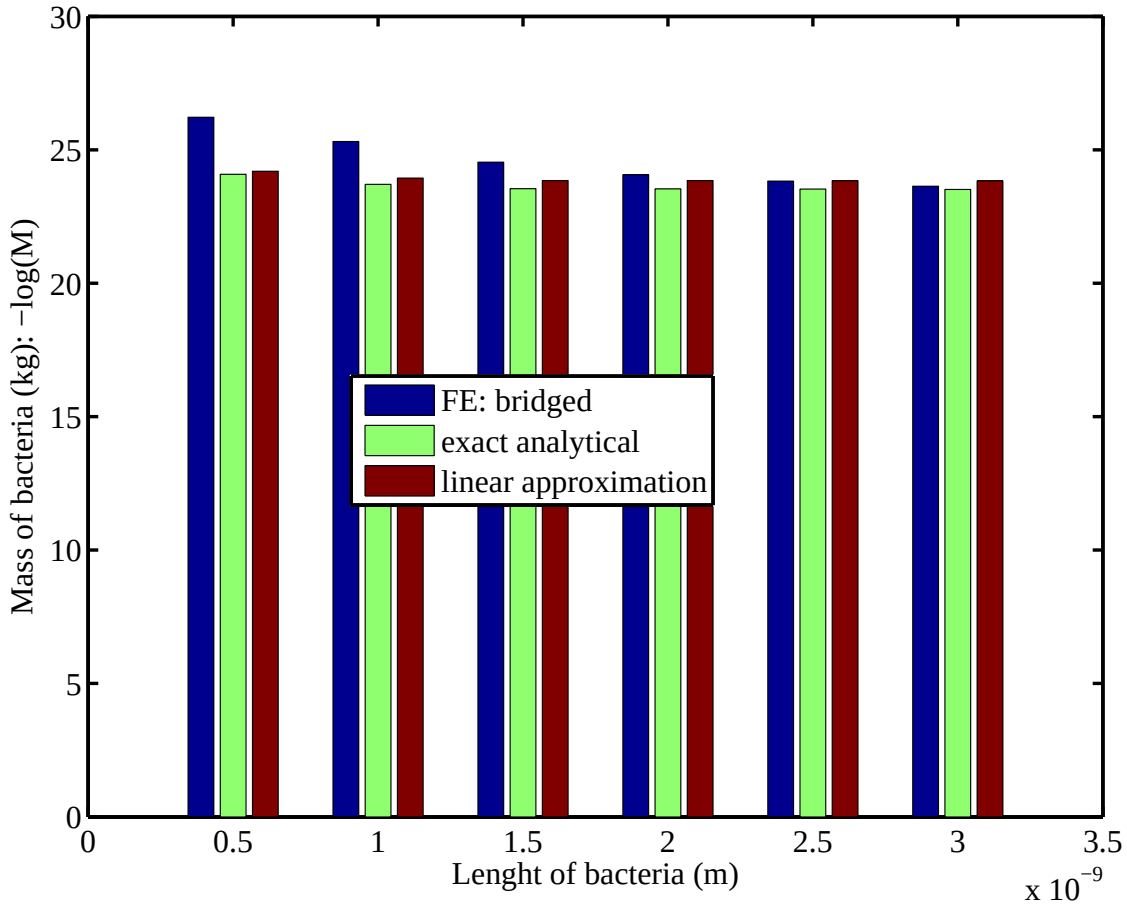

The variation of identified mass with bacterial length using the finite element simulation, exact analytical formula and the linear approximation for the bridged nanotube. Proposed analytical expressions are in good agreement with the detailed finite element results for longer bacterial length.

Validation of sensor equations

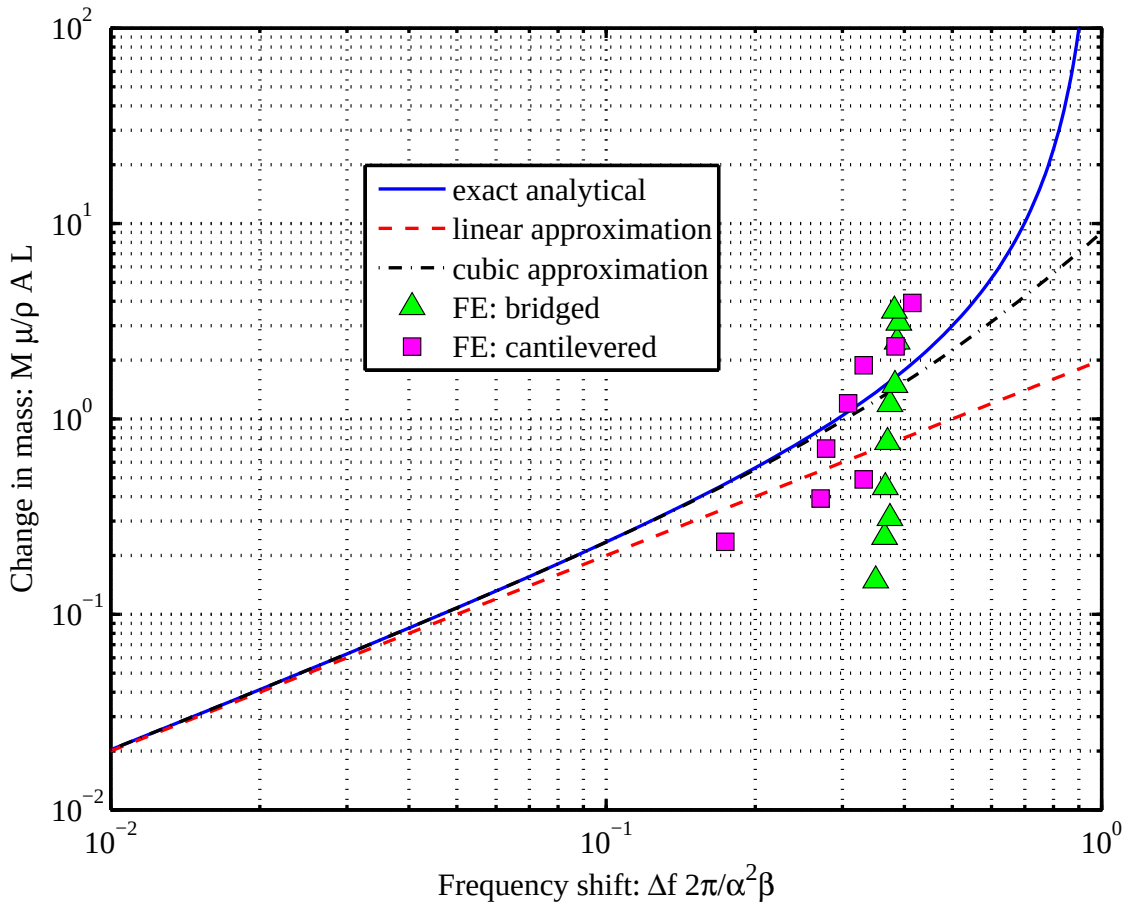

The general relationship between the normalized frequency-shift and normalized added mass of the bio-particles in a SWCNT with effective density ρ, cross-section area A and length L. Relationship between the frequency-shift and added mass of bio-particles obtained from finite element simulation are also presented here to visualize the effectiveness of analytical formulas.

Nonlocal Resonance Frequency of CNT with Attached Biomolecule

- We consider the frequency of carbon nanotubes (CNT) with attached mass, for example, deoxythymidine molecule

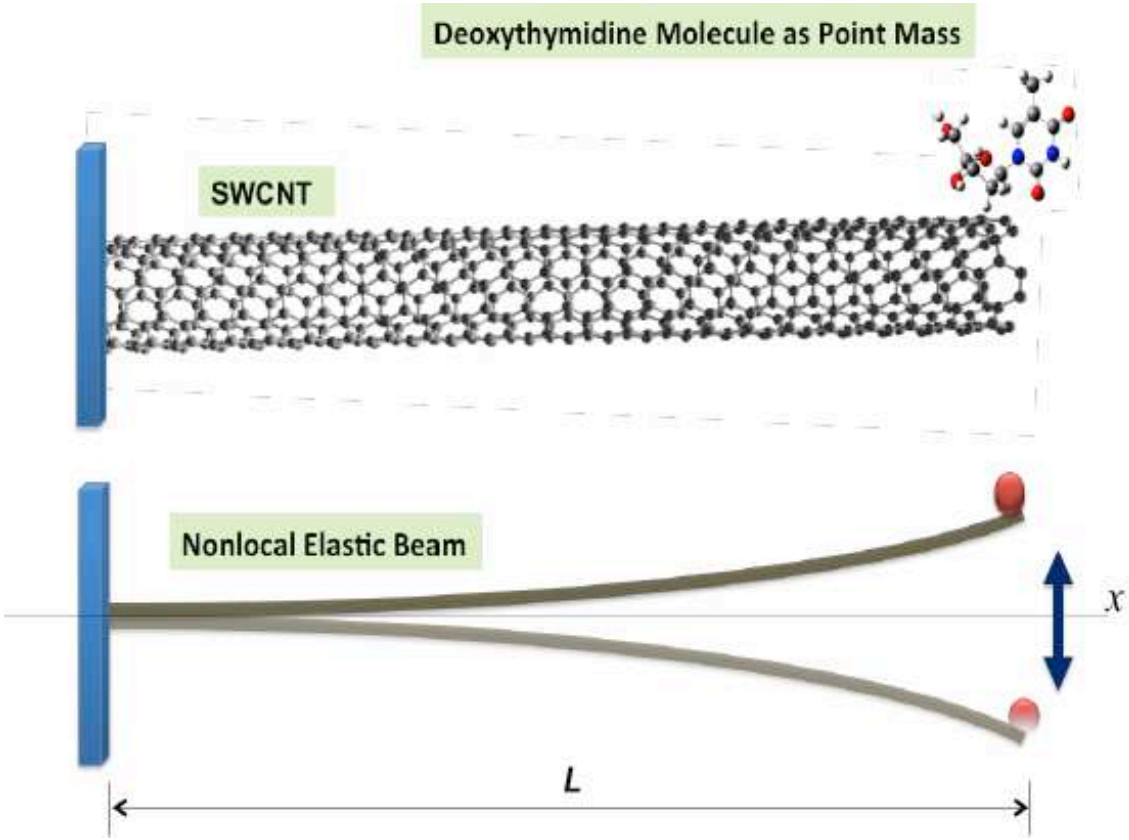

Nonlocal Resonance Frequency of CNT with Attached biomolecule

- For the bending vibration of a nonlocal damped beam, the equation of motion of free vibration can be expressed by

$$EI\frac{\partial^4 V(x,t)}{\partial x^4} + m\left(1-(e_0 a)^2\frac{\partial^2}{\partial x^2}\right)\left\{\frac{\partial^2 V(x,t)}{\partial t^2}\right\} = 0 \tag{65}$$

- In the fundamental mode of vibration, the natural frequency of a nonlocal SWCNT oscillator can be expressed as

$$f_n = \frac{1}{2\pi}\sqrt{\frac{k_{eq}}{m_{eq}}} \tag{66}$$

Here k_{eq} and m_{eq} are respectively equivalent stiffness and mass of SWCNT in the first mode of vibration.

Nonlocal resonance frequency with attached point biomolecule

- Following the energy approach, the natural frequency can be expressed as

$$f_n = \frac{1}{2\pi}\sqrt{\frac{k_{eq}}{m_{eq}}} = \frac{\beta}{2\pi}\frac{c_k}{\sqrt{1 + c_{nl}\theta^2 + c_m\Delta M}} \tag{67}$$

where

$$\beta = \sqrt{\frac{EI}{\rho A L^4}}, \theta = \frac{e_0 a}{L} \quad \text{and} \quad \Delta M = \frac{M}{\rho A L} \tag{68}$$

- The stiffness, mass and nonlocal calibration constants are

$$c_k = \sqrt{\frac{140}{11}}, c_m = \frac{140}{33} \quad \text{and} \quad c_{nl} = \frac{56}{11} \tag{69}$$

Equation (67), together with the calibration constants gives an explicit relationship between the change in the mass and frequency.

Nonlocal resonance frequency with attached distributed biomolecules

- We consider the frequency of carbon nanotubes (CNT) with attached distributed mass, for example, a collections of deoxythymidine molecules

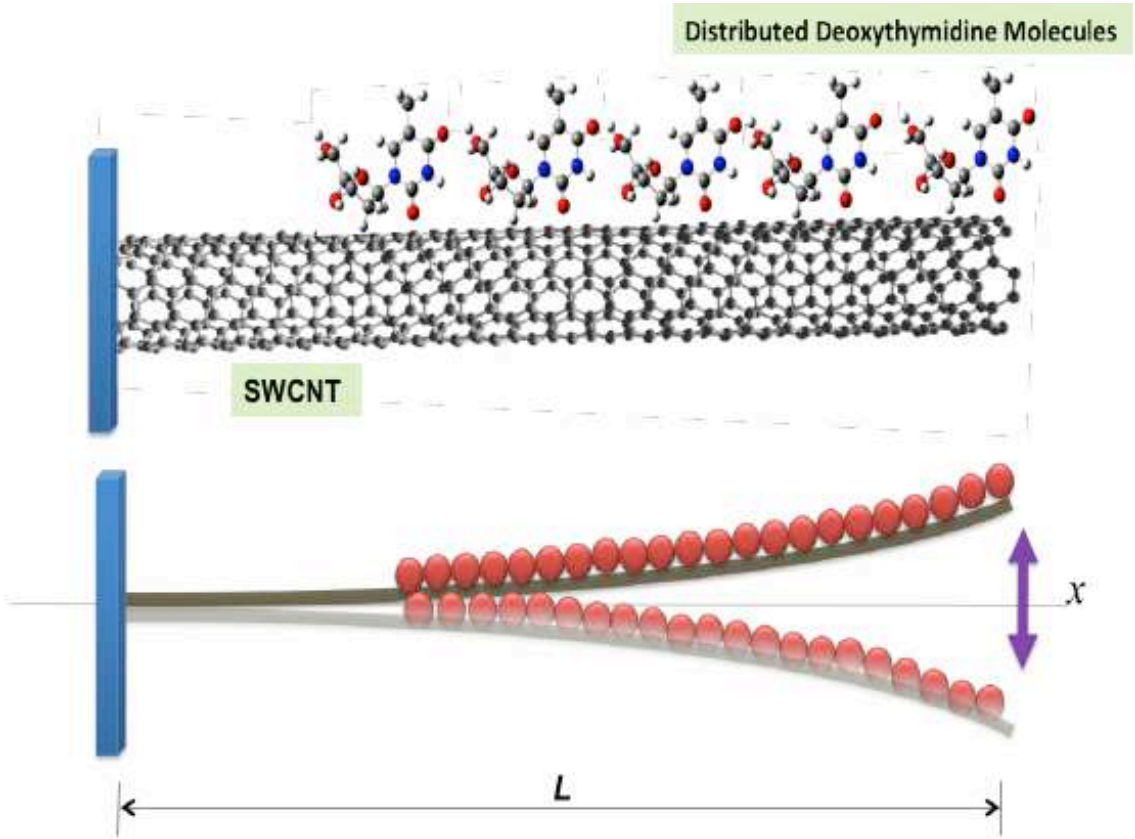

Nonlocal resonance frequency with attached distributed biomolecules

- Following the energy approach, the natural frequency can be expressed as

$$f_n = \frac{1}{2\pi}\sqrt{\frac{k_{eq}}{m_{eq}}} = \frac{\beta}{2\pi}\frac{c_k}{\sqrt{1 + c_{nl}\theta^2 + c_m(\gamma)\Delta M}} \tag{70}$$

where

$$\beta = \sqrt{\frac{EI}{\rho A L^4}}, \theta = \frac{e_0 a}{L}, \Delta M = \frac{M}{\rho A L}, c_k = \sqrt{\frac{140}{11}} \quad \text{and} \quad c_{nl} = \frac{56}{11} \tag{71}$$

- The length-dependent mass calibration constant is

$$c_m(\gamma) = \frac{140 - 210\gamma + 105\gamma^2 + 35\gamma^3 - 42\gamma^4 + 5\gamma^6}{33} \tag{72}$$

Equation (70), together with the calibration constants gives an explicit relationship between the change in the mass and frequency.

Nonlocal sensor equations

- The resonant frequency of a SWCNT with no added mass is obtained by substituting $\Delta M = 0$ in Eq. (70) as

$$f_{0_n} = \frac{1}{2\pi} c_k \beta \tag{73}$$

- Combining equations (70) and (73) one obtains the relationship between the resonant frequencies as

$$f_n = \frac{f_{0_n}}{\sqrt{1 + c_{nl}\theta^2 + c_m(\gamma)\Delta M}} \tag{74}$$

- The frequency-shift can be expressed using Eq. (74) as

$$\Delta f = f_{0_n} - f_n = f_{0_n} - \frac{f_{0_n}}{\sqrt{1 + c_{nl}\theta^2 + c_m(\gamma)\Delta M}} \tag{75}$$

- From this we obtain

$$\frac{\Delta f}{f_{0_n}} = 1 - \frac{1}{\sqrt{1 + c_{nl}\theta^2 + c_m(\gamma)\Delta M}} \tag{76}$$

Nonlocal sensor equations

- Rearranging gives the expression

Relative mass detection

$$\Delta M = \frac{1}{c_m(\gamma)\left(1-\frac{\Delta f}{f_{0_n}}\right)^2} - \frac{c_{nl}}{c_m(\gamma)}\theta^2 - \frac{1}{c_m(\gamma)} \tag{77}$$

- This equation completely relates the change in mass with the frequency-shift using the mass calibration constant. The actual value of the added mass can be obtained from (77) as

Absolute mass detection

$$M = \frac{\rho AL}{c_m(\gamma)}\frac{\left(c_k^2\beta^2\right)}{\left(c_k\beta - 2\pi\Delta f\right)^2} - \frac{c_{nl}}{c_m(\gamma)}\theta^2\rho AL - \frac{\rho AL}{c_m(\gamma)} \tag{78}$$

This is the general equation which completely relates the added mass and the frequency shift using the calibration constants.

Zigzag (5,0) SWCNT of length 8.52 nm with added DeOxy Thymidine (a nucleotide that is found in DNA)

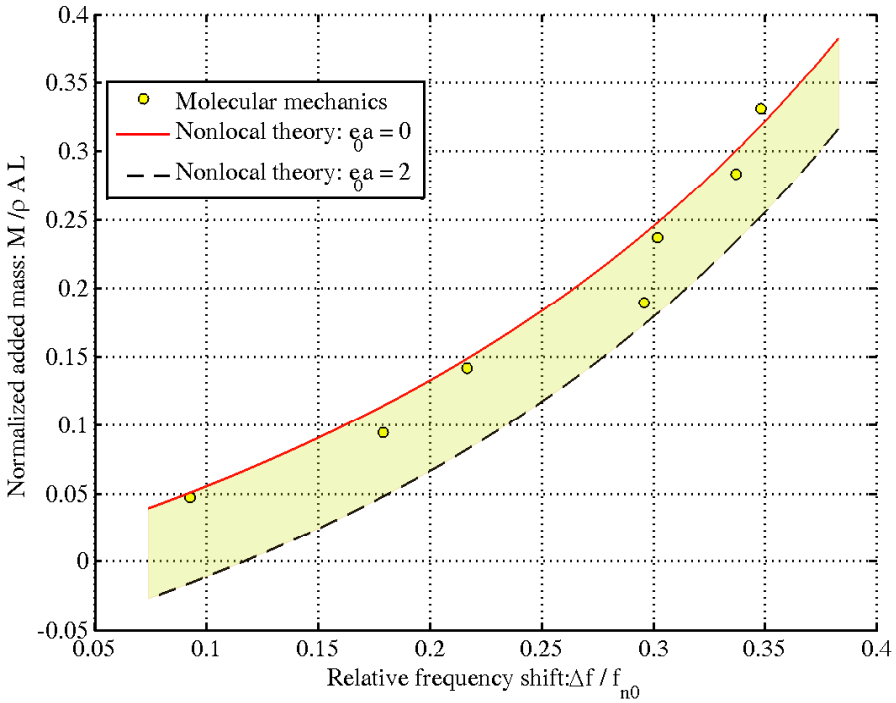

(a) Point mass on a cantilevered CNT.

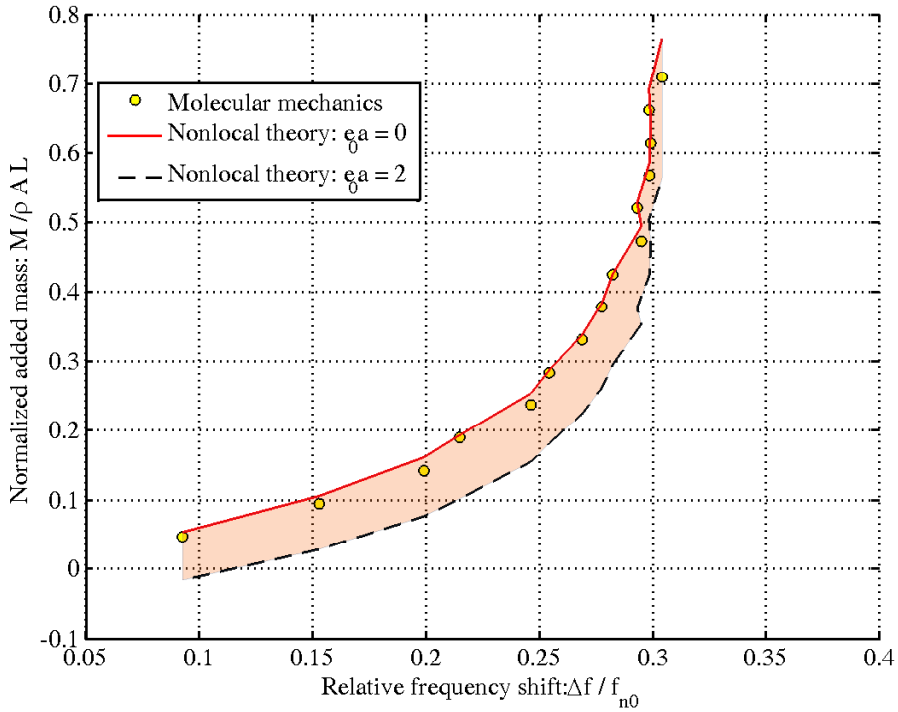

(b) Distributed mass on a cantilevered CNT. The length of the mass varies between $0.05L$ to $0.72L$ from the edge of the CNT.

Figure: Normalized mass vs. relative frequency shift for the SWCNT with point mass. The band covers the complete range of nonlocal the parameter $0 \leq e_2 \leq 2$nm. It can be seen that the molecular mechanics simulation results reasonably fall within this band (except at $\Delta f / f_{n0}$=0.35).

Results for optimal values of the nonlocal parameter

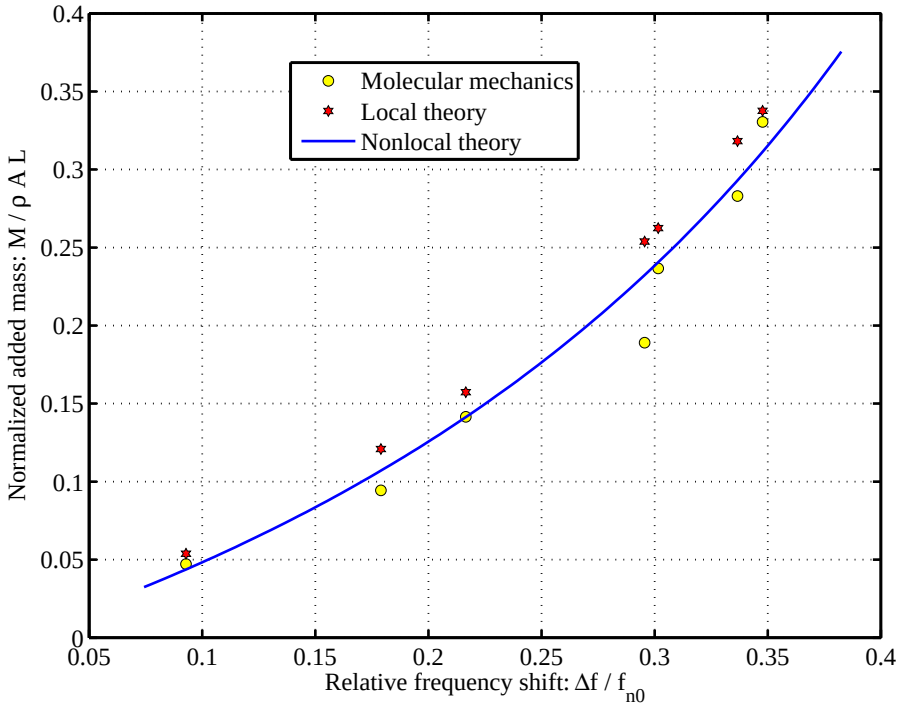

(a) Point mass on a cantilevered CNT: $e_0 a = 0.65$nm.

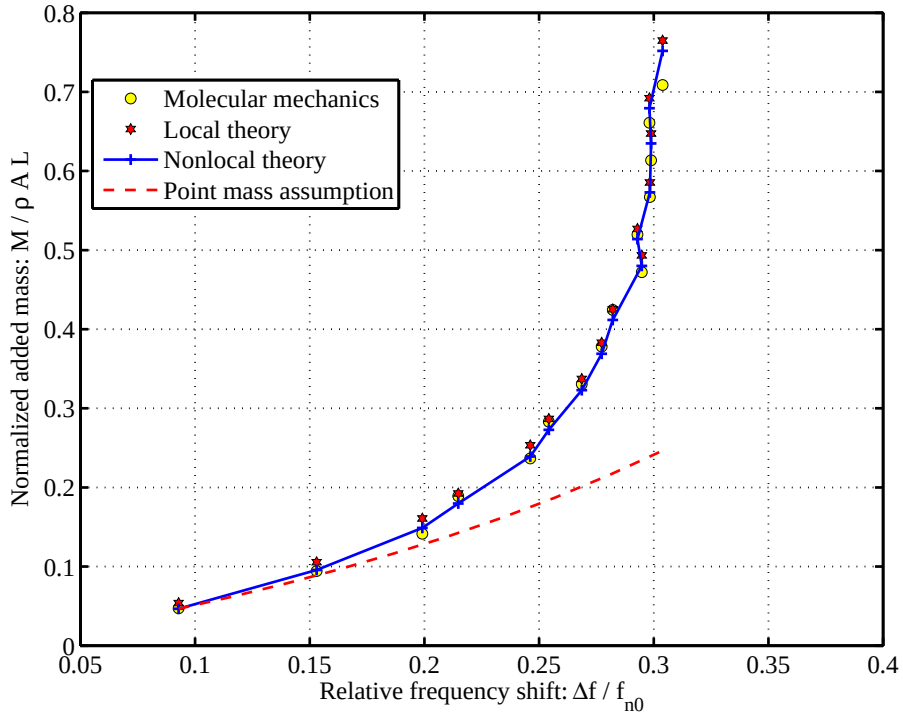

(b) Distributed mass on a cantilevered CNT. $e_0 a = 0.5$nm.

Figure: Normalized mass vs. relative frequency shift for the SWCNT with point mass with optimal values of the nonlocal parameter $e_0 a$.

Error in mass detection: point mass

Percentage error in the mass detection using cantilevered CNT based biosensors for single biomolecule. The errors are shown for both local and nonlocal elastic theories (with optimised nonlocal parameter $e_0 a = 0.65$ nm).

Relative frequency shift	Percentage error	
	Local elasticity	Nonlocal elasticity
0.0929	13.9879	7.3226
0.179	28.1027	13.3841
0.2165	11.1765	0.1131
0.2956	34.2823	22.9147
0.3016	10.9296	1.6392
0.3367	12.4422	3.5486
0.3477	2.1427	5.807

Error in mass detection: distributed mass

Percentage errors in the mass detection using cantilevered CNT based biosensor for distributed added biomolecules. The errors are shown for both local and nonlocal elastic theories (with optimised nonlocal parameter $e_0 a = 0.5$ nm).

Relative frequency shift	Normalized length	Percentage error	
		Local elasticity	Nonlocal elasticity
0.0929	0	13.9879	1.2813
0.153	0.05	11.8626	1.4132
0.1991	0.1	13.7038	5.171
0.2148	0.15	1.7865	4.9412
0.2462	0.2	7.0172	1.0914
0.2542	0.25	1.3278	3.6149
0.2687	0.3	1.9943	2.2774
0.2773	0.35	1.2631	2.4081
0.2821	0.4	0.1653	3.0046
0.2948	0.45	4.515	1.7056
0.2929	0.5	1.3776	1.0761
0.2983	0.55	3.2275	1.0155
0.2989	0.6167	5.524	3.4922
0.2981	0.6667	4.6735	2.7585
0.3039	0.7167	7.9455	6.0986

Nonlocal plate theory for single-layer graphene sheets (SLGS)

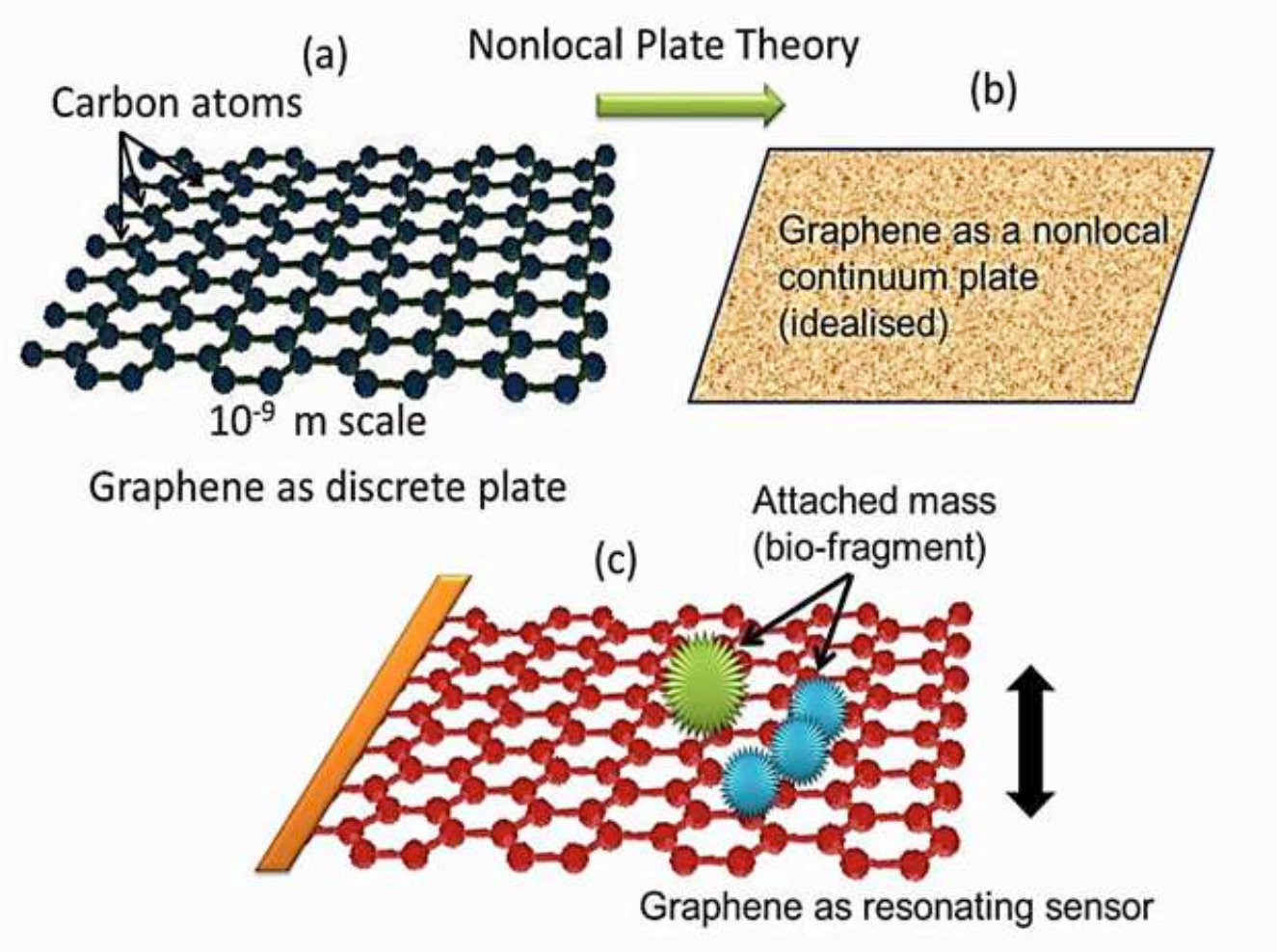

(a) Schematic diagram of single-layer graphene sheets, (b) Nonlocal continuum plate as a model for graphene sheets, (c) Resonating graphene sheets sensors with attached bio fragment molecules such as adenosine.

Nonlocal plate theory for SLGS

- We model SLGS dynamics as a thin nonlocal plate in transverse vibration

$$D\nabla^4 u + m\left(1 - (e_0 a)^2\nabla^2\right)\left\{\frac{\partial^2 u}{\partial t^2}\right\}, \tag{79}$$
$$0 \leq x \leq c;\ 0 \leq y \leq b.$$

- Here $u \equiv u(x, y, t)$ is the transverse deflection, $\nabla^2 = \left(\frac{\partial^2}{\partial x^2} + \frac{\partial^2}{\partial y^2}\right)$ is the differential operator, x, y are coordinates, t is the time, ρ is the mass density per area and the bending rigidity is defined by

$$D = \frac{Eh^3}{12(1-\nu^2)} \tag{80}$$

- Introducing the non dimensional length scale parameter

$$\mu = \frac{e_0 a}{c} \tag{81}$$

the resonance frequency can be obtained as

$$\omega_0^2 = \left(\frac{\pi^4 D}{c^4 \rho}\right)\frac{1/32}{(3\pi - 8)/2\pi + \mu^2\pi^2/8} \tag{82}$$

Nonlocal SLGS with attached masses

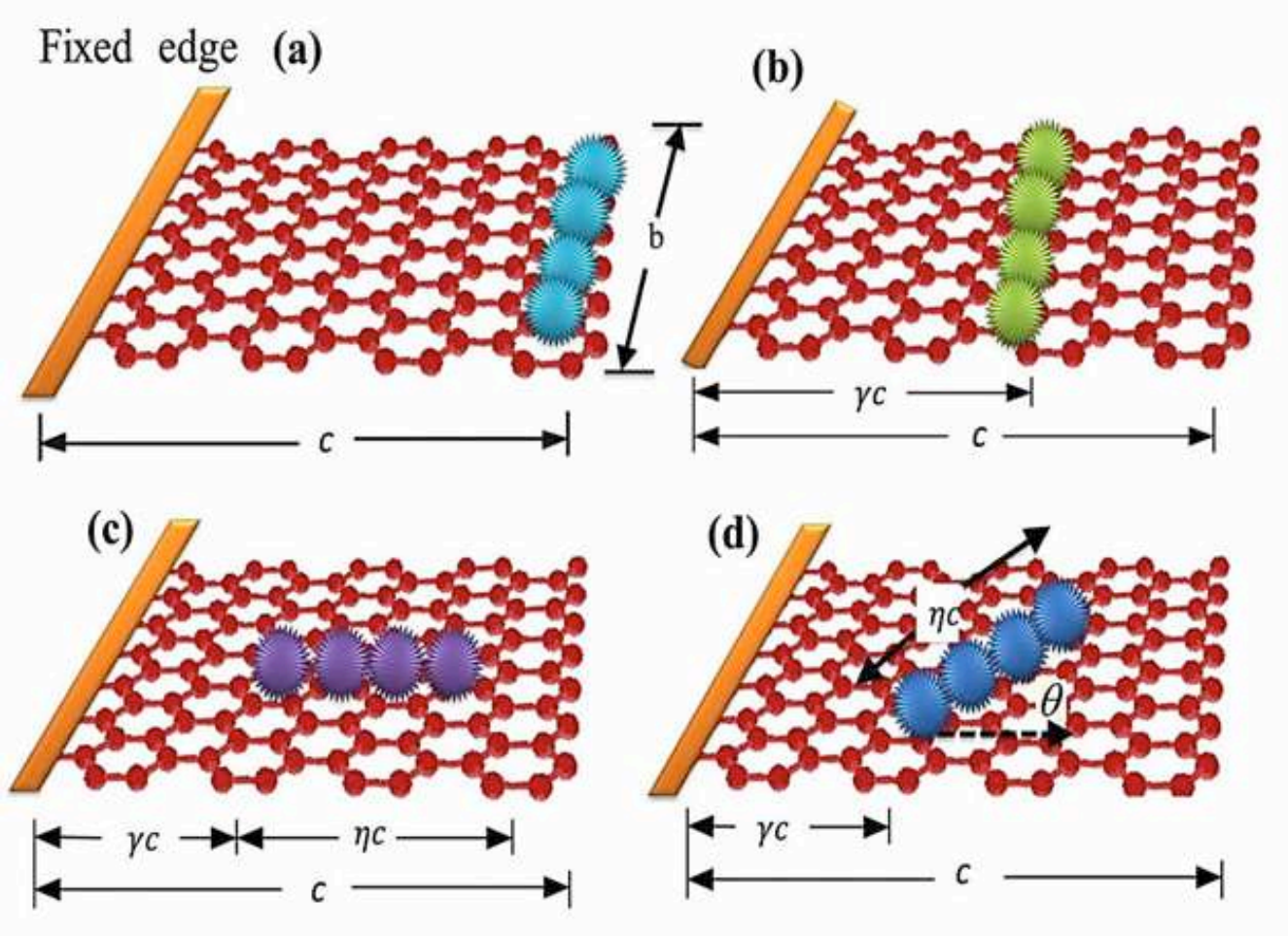

(a) Masses at the cantilever tip in a line (b) masses in a line along the width, (c) masses in a line along the length, (d) masses in a line with an arbitrary angle.

Nonlocal resonant frequencies of SLGS with attached mass

- Using the energy approach, the resonance frequency can be expressed in a general form as

$$\omega^2_{a,b,c,d} = \frac{\frac{1}{2}\frac{\pi^4 D}{c^3} b(1/32)}{\frac{1}{2}\left\{cb\rho\left(\frac{3\pi-8}{2\pi} + \frac{\mu^2\pi^2}{8}\right) + \alpha_{a,b,c,d} M\right\}}$$
$$= \left(\frac{\pi^4 D}{c^4\rho}\right) \frac{1/32}{(3\pi-8)/2\pi + \mu^2\pi^2/8 + \beta\alpha_{b,c,d}} \tag{83}$$

- Here the ratio of the added mass

$$\beta = \frac{M}{M_g} \tag{84}$$

and $\alpha_{b,c,d}$ are factors which depend on the mass distribution as defined before.

Free vibration response of nonlocal SLGS with attached masses

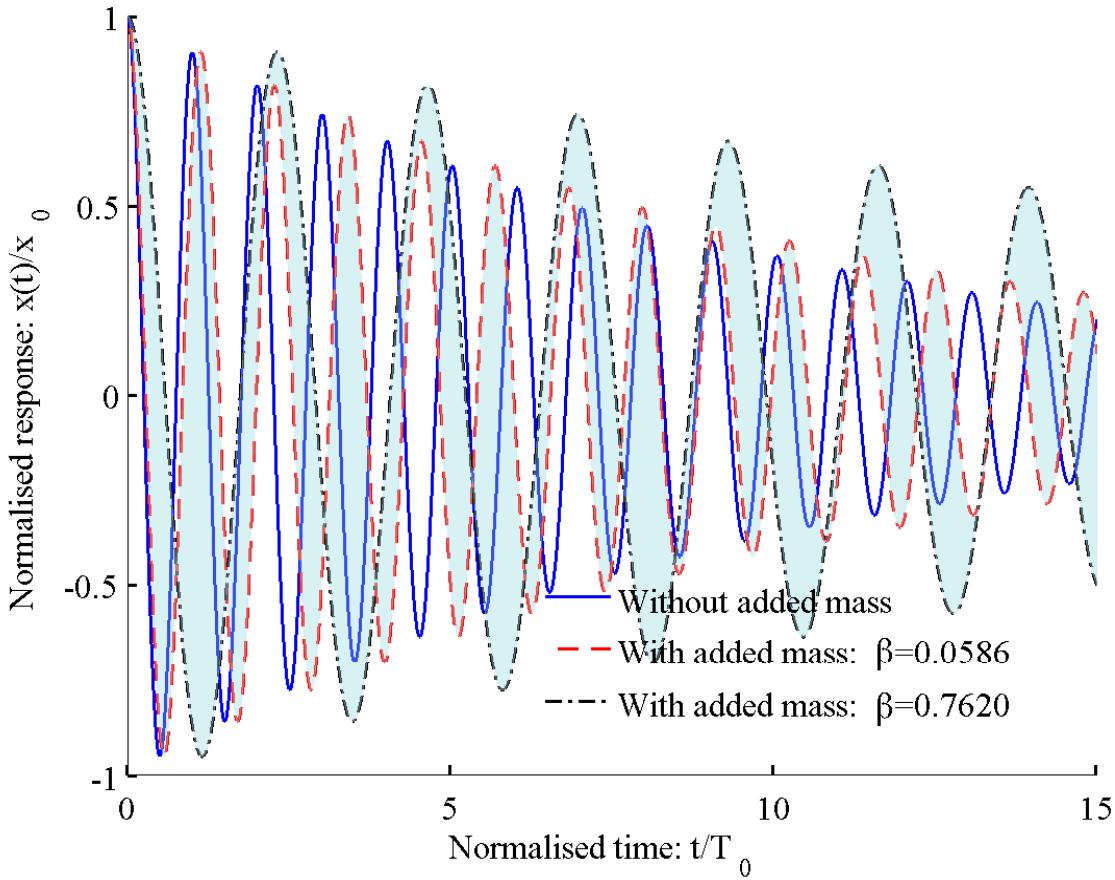

Free vibration response at the tip of the graphene sheet due to the unit initial displacement obtained from molecular mechanics simulation. Here T_0 is the time period of oscillation without any added mass. The shaded area represents the motion of all the mass loading cases considered for case (a).

Validation with MM simulation (UFF): Case a

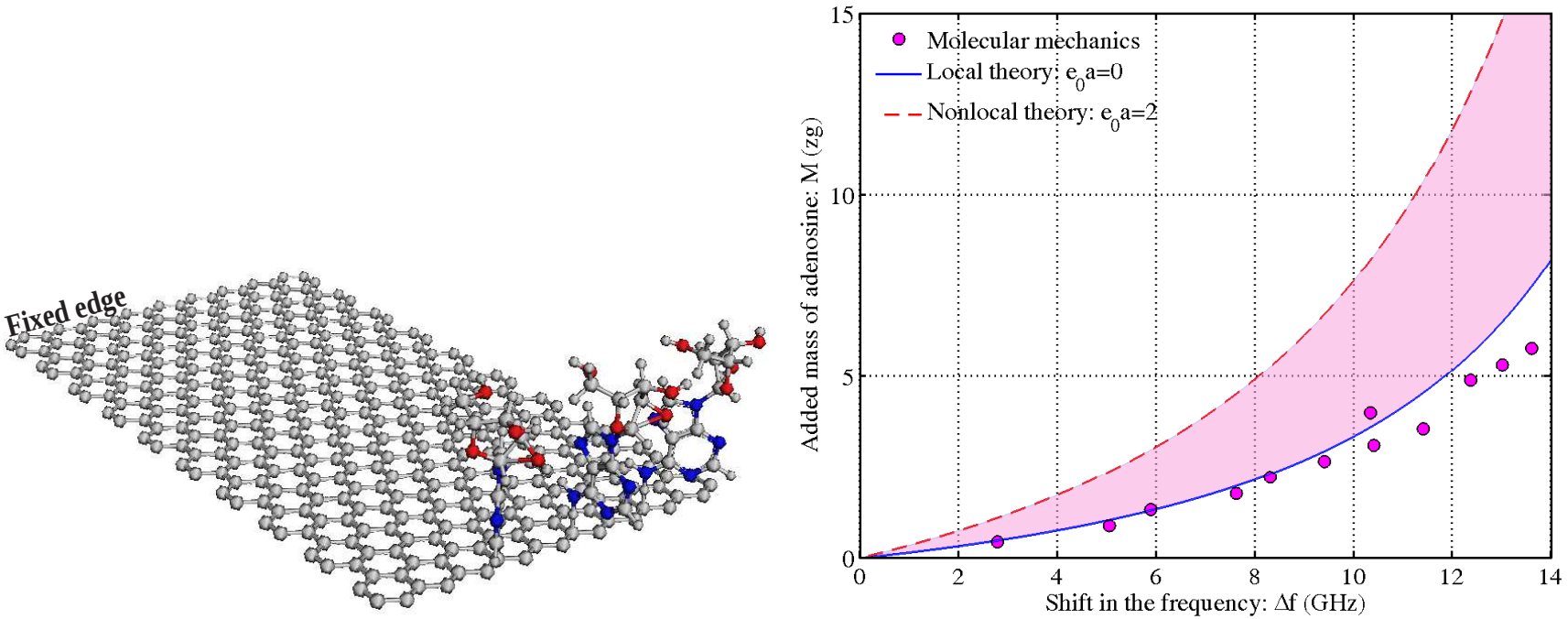

(a) SLGS with adenosine molecules at the cantilever tip in a line

(b) Identified mass from the frequency shift

Figure: Identified attached masses from the frequency-shift of a cantilevered SLGS resonator for case (a). The SLGS mass is 7.57zg and the mass of each adenosine molecule is 0.44zg. The proposed approach is validated using data from the molecular mechanics simulations. Up to 12 adenosine molecules are attached to the graphene sheet.

Validation with MM simulation: Case b

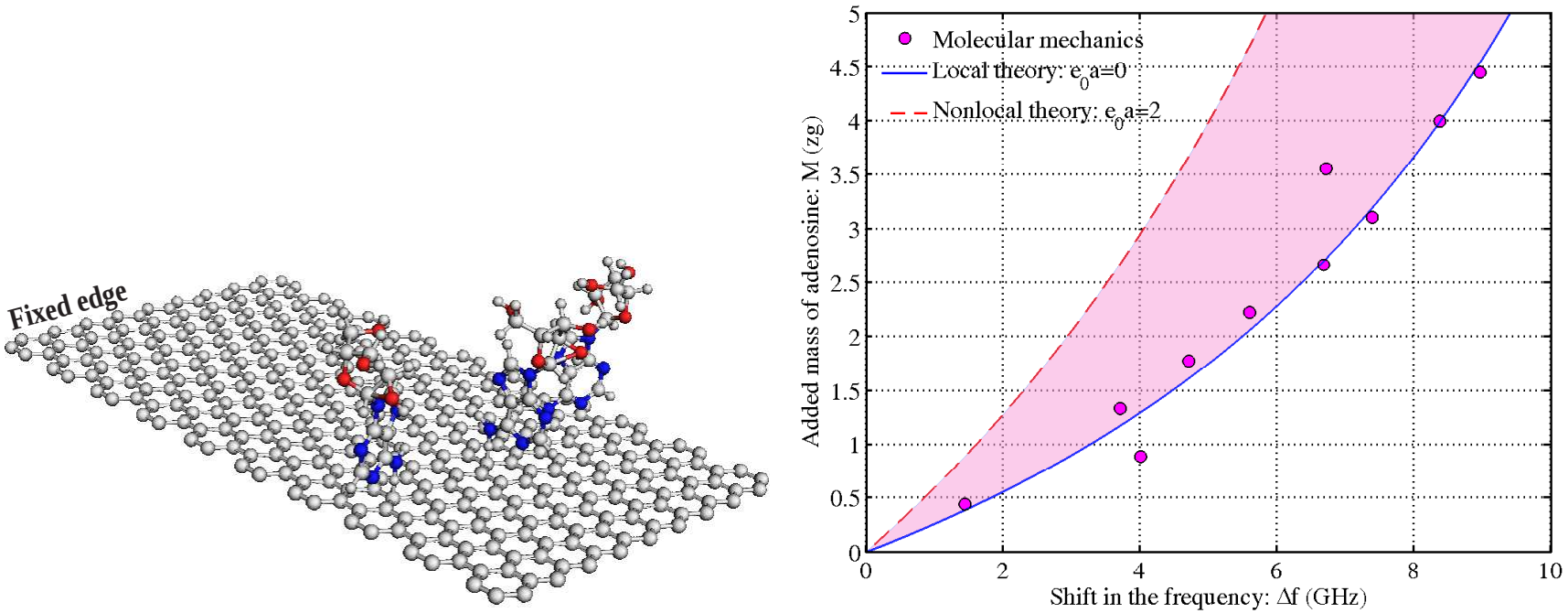

(a) SLGS with adenosine molecules in a line along the width

(b) Identified mass from the frequency shift, $\gamma = 0.85$

Figure: Identified attached masses from the frequency-shift of a cantilevered SLGS resonator for case (b). The proposed approach is validated using data from the molecular mechanics simulations. Up to 10 adenosine molecules are attached to the graphene sheet.

Validation with MM simulation: Case d

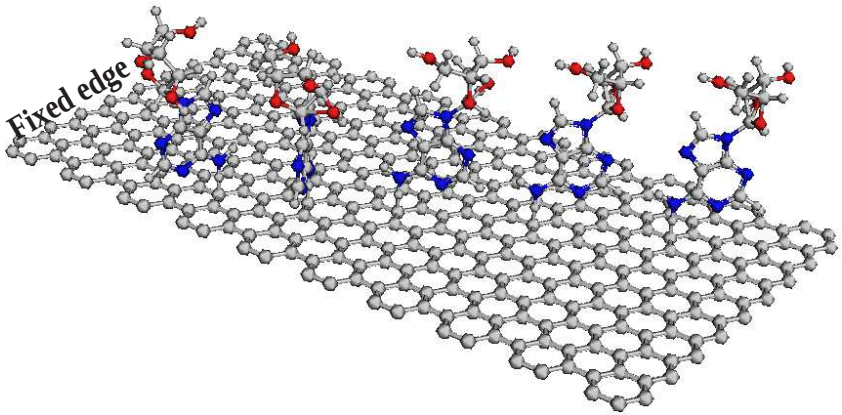

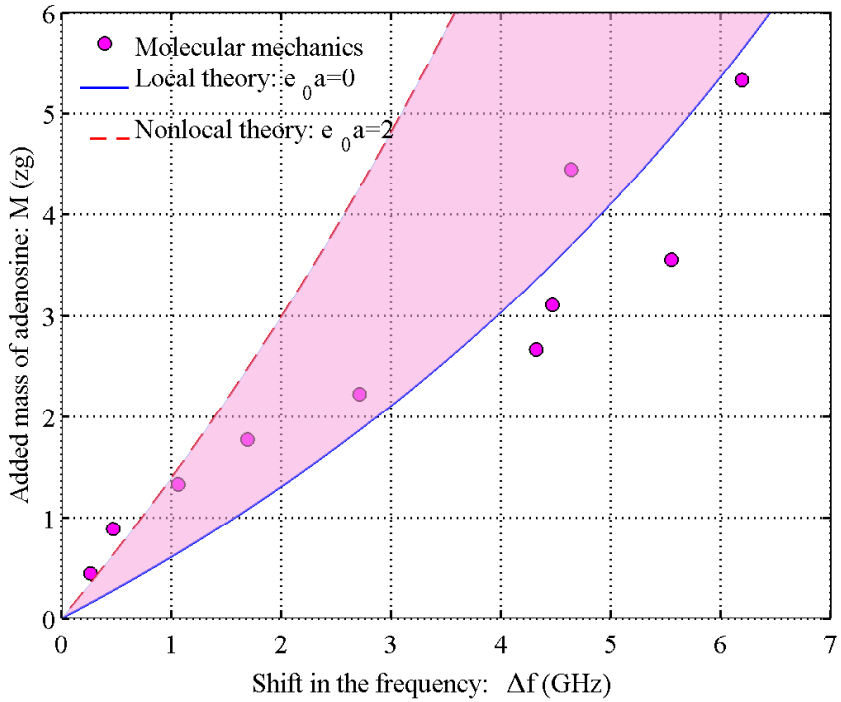

(a) SLGS with adenosine molecules in a line with an arbitrary angle

(b) Identified mass from the frequency shift, $\gamma = 0.25$, $\eta = 0.7$ and $\theta = \pi/6$

Figure: Identified attached masses from the frequency-shift of a cantilevered SLGS resonator for case (d). The proposed approach is validated using data from the molecular mechanics simulations. Up to 10 adenosine molecules are attached to the graphene sheet.

Conclusions

- The natural frequencies and the dynamic response obtained using the conventional finite element approach were compared with the results obtained using the dynamic finite method.
- Good agreement between the two methods was found for small values of the nonlocal parameter.
- For larger values of the nonlocal parameter, the conventional finite element approach is unable to capture the dynamics due to very high modal density near to the maximum frequency.
- In this case the proposed dynamic finite element approach provides a simple and robust alternative.

Conclusions

- Principles of fundamental mechanics and dynamics can have unprecedented role in the development of nano-mechanical bio sensors. Nano-sensor market is predicted to be over 20 Billion$ by 2020.
- Mass sensing is an inverse problem - NOT a conventional "forward problem".
- Due to the need for "instant calculation", physically insightful simplified (but approximate) approach is more suitable compared to very detailed (but accurate) molecular dynamic simulations.
- Energy based simplified dynamic approach turned out to sufficient to identify mass of the attached bio-objects from "measured" frequency-shifts in nano-scale sensors.
- Closed-form sensor equations have been derived and independently validated using molecular mechanics simulations. Calibration constants necessary for this approach have been given explicitly for point mass as well as distributed masses.
- Nonlocal model with optimally selected length-scale parameter improves the mass detection capability for nano-sensors.

Further reading

[1] M. Aydogdu, Axial vibration of the nanorods with the nonlocal continuum rod model, Physica E 41 (5) (2009) 861–864.
[2] S. Filiz, M. Aydogdu, Axial vibration of carbon nanotube heterojunctions using nonlocal elasticity, Computational Materials Science 49 (3) (2010) 619–627.
[3] S. Narendar, S. Gopalakrishnan, Non local scale effects on ultrasonic wave characteristics nanorods, Physica E-Low-Dimensional Systems & Nanostructures 42 (5) (2010) 1601–1604.
[4] T. Murmu, S. Adhikari, Nonlocal effects in the longitudinal vibration of double-nanorod systems, Physica E: Low-dimensional Systems and Nanostructures 43 (1) (2010) 415–422.
[5] S. C. Pradhan, Buckling of single layer graphene sheet based on nonlocal elasticity and higher order shear deformation theory, Physics Letters A 373 (45) (2009) 4182–4188.
[6] P. Malekzadeh, A. R. Setoodeh, A. A. Beni, Small scale effect on the free vibration of orthotropic arbitrary straight-sided quadrilateral nanoplates, Composite Structures 93 (7) (2011) 1631–1639.
[7] R. D. Firouz-Abadi, M. M. Fotouhi, H. Haddadpour, Free vibration analysis of nanocones using a nonlocal continuum model, Physics Letters A 375 (41) (2011) 3593–3598.
[8] A. A. Pisano, A. Sofi, P. Fuschi, Nonlocal integral elasticity: 2d finite element based solutions, International Journal of Solids and Structures 46 (21) (2009) 3836–3849.
[9] J. K. Phadikar, S. C. Pradhan, Variational formulation and finite element analysis for nonlocal elastic nanobeams and nanoplates, Computational Materials Science 49 (3) (2010) 492–499.
[10] J. F. Doyle, Wave Propagation in Structures, Springer Verlag, New York, 1989.
[11] M. Paz, Structural Dynamics: Theory and Computation, 2nd Edition, Van Nostrand, Reinhold, 1980.
[12] J. R. Banerjee, F. W. Williams, Exact bernoulli-euler dynamic stiffness matrix for a range of tapered beams, International Journal for Numerical Methods in Engineering 21 (12) (1985) 2289–2302.
[13] J. R. Banerjee, Coupled bending torsional dynamic stiffness matrix for beam elements, International Journal for Numerical Methods in Engineering 28 (6) (1989) 1283–1298.
[14] J. R. Banerjee, F. W. Williams, Coupled bending-torsional dynamic stiffness matrix for timoshenko beam elements, Computer and Structures 42 (3) (1992) 301–310.
[15] J. R. Banerjee, S. A. Fisher, Coupled bending torsional dynamic stiffness matrix for axially loaded beam elements, International Journal for Numerical Methods in Engineering 33 (4) (1992) 739–751.
[16] N. J. Ferguson, W. D. Pilkey, Literature review of variants of dynamic stiffness method, Part 1: The dynamic element method, The Shock and Vibration Digest 25 (2) (1993) 3–12.
[17] N. J. Ferguson, W. D. Pilkey, Literature review of variants of dynamic stiffness method, Part 2: Frequency-dependent matrix and other, The Shock and Vibration Digest 25 (4) (1993) 3–10.
[18] J. R. Banerjee, F. W. Williams, Free-vibration of composite beams - an exact method using symbolic computation, Journal of Aircraft 32 (3) (1995) 636–642.
[19] C. S. Manohar, S. Adhikari, Dynamic stiffness of randomly parametered beams, Probabilistic Engineering Mechanics 13 (1) (1998) 39–51.
[20] J. R. Banerjee, Dynamic stiffness formulation for structural elements: A general approach, Computer and Structures 63 (1) (1997) 101–103.
[21] S. Adhikari, C. S. Manohar, Transient dynamics of stochastically parametered beams, ASCE Journal of Engineering Mechanics 126 (11) (2000) 1131–1140.
[22] S. Gopalakrishnan, A. Chakraborty, D. R. Mahapatra, Spectral Finite Element Method, Springer Verlag, New York, 2007.

[23] S. M. Hashemi, M. J. Richard, G. Dhatt, A new Dynamic Finite Element (DFE) formulation for lateral free vibrations of Euler-Bernoulli spinning beams using trigonometric shape functions, Journal of Sound and Vibration 220 (4) (1999) 601–624.
[24] S. M. Hashemi, M. J. Richard, Free vibrational analysis of axially loaded bending-torsion coupled beams: a dynamic finite element, Computer and Structures 77 (6) (2000) 711–724.
[25] J. N. Reddy, Nonlocal theories for bending, buckling and vibration of beams, International Journal of Engineering Science 45 (2-8) (2007) 288–307.
[26] A. Eringen, On differential-equations of nonlocal elasticity and solutions of screw dislocation and surface waves, Journal of Applied Physics 54 (9) (1983) 4703–4710.
[27] L. Meirovitch, Principles and Techniques of Vibrations, Prentice-Hall International, Inc., New Jersey, 1997.
[28] T. Murmu, S. Adhikari, Nonlocal vibration of carbon nanotubes with attached buckyballs at tip, Mechanics Research Communications 38 (1) (2011) 62–67.
[29] M. Petyt, Introduction to Finite Element Vibration Analysis, Cambridge University Press, Cambridge, UK, 1998.
[30] D. Dawe, Matrix and Finite Element Displacement Analysis of Structures, Oxford University Press, Oxford, UK, 1984.
[31] S. Adhikari, Doubly spectral stochastic finite element method (dssfem) for structural dynamics, ASCE Journal of Aerospace Engineering 24 (3) (2011) 264–276.